QEX

May/June 2022

www.arrl.org

A Forum for Communications Experimenters

Issue No. 332

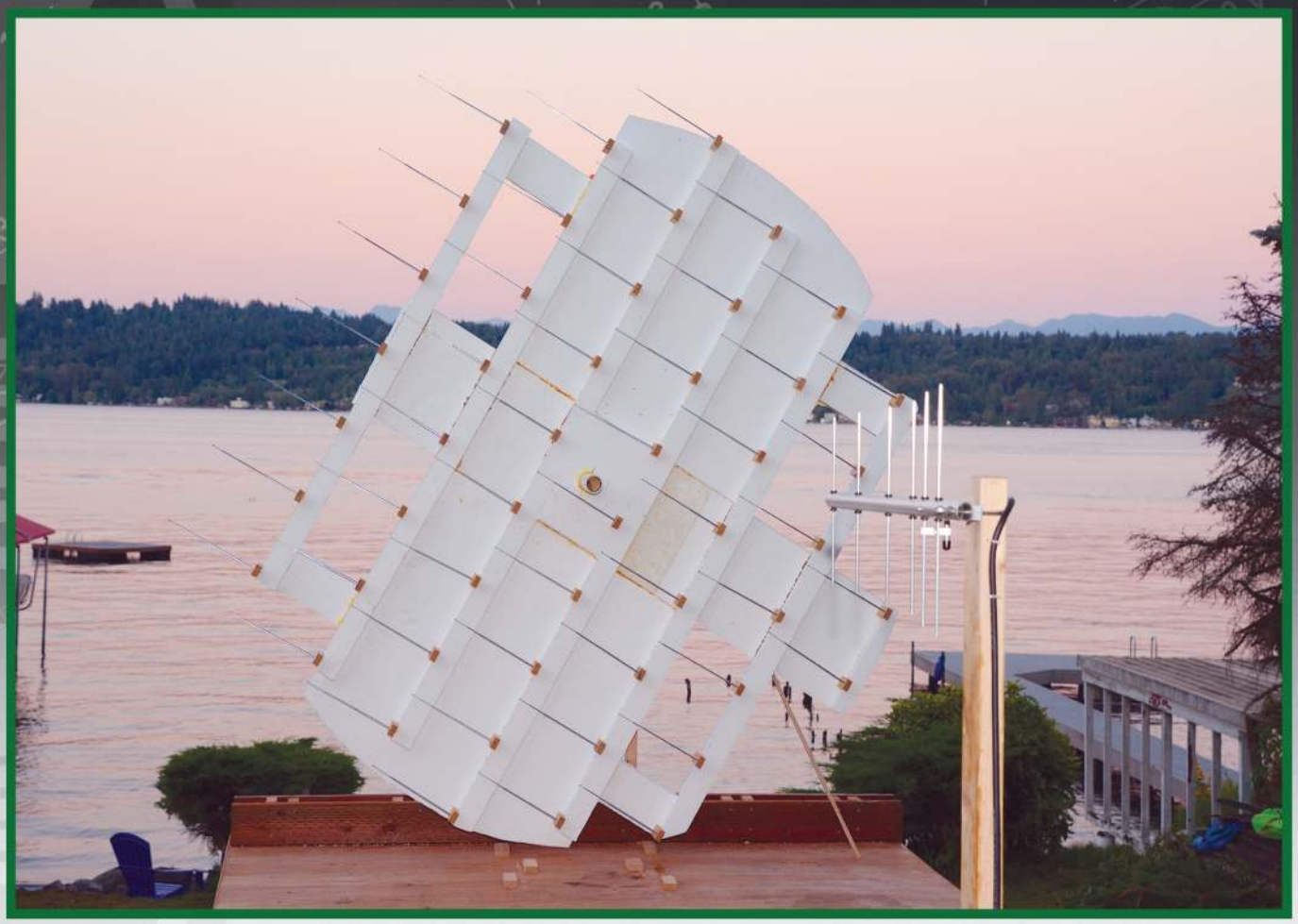

Meredith Hillier, KG7EUM, and David Hillier, AA7XX, measure the effects of metal obstructions on radio wave propagation.

The EVENT HORIZON OF DX

TS-990S

Dual TFT Display & Dual Receiver HF/50 MHz Transceiver

The main receiver has an IP3 in the +40 dB class, and the sub receiver is the already famous TS-590S receiver. Capable of receiving two signals at once, on different bands. 7-inch and 3.5-inch color TFT displays allow displaying of independent contents. Simplification of complex operations at a glance. Make no mistake, this is not a toy. Finally a serious tool is available for getting the very most from your hobby, of course it's a Kenwood.

- Covers the HF and 50 MHz bands.
- High-speed automatic antenna tuner.
- USB, Serial and LAN ports.
- Various PC applications (free software): ARCP-990 enabling PC control, ARHP-990 enabling remote control, and ARUA-10 USB audio driver.
- Clean 5 to 200 W transmit power through the 50 V FET final unit.
- Built-in RTTY and PSK.
- Three Analog Devices 32-bit floating-point arithmetic DSPs.
- DVI output for display by an external monitor (main screen display only).

KENWOOD

Customer Support: (310) 639-4200
Fax: (310) 537-8235

www.kenwood.com/usa

ISO9001 Registered

ADS#05421

QEX (ISSN: 0886-8093) is published bimonthly in January, March, May, July, September, and November by the American Radio Relay League, 225 Main St., Newington, CT 06111-1400. Periodicals postage paid at Hartford, CT and at additional mailing offices.

POSTMASTER: Send address changes to: QEX, 225 Main St., Newington, CT 06111-1400
Issue No. 332

Publisher
American Radio Relay League

Kazimierz "Kai" Siwiak, KE4PT
Editor

Lori Weinberg, KB1EIB
Assistant Editor

Scotty Cowling, WA2DFI
Ray Mack, W5IFS
Contributing Editors

Production Department

Becky R. Schoenfeld, W1BXY
Publications Manager

Michelle Bloom, WB1ENT
Production Supervisor

David Pingree, N1NAS
Senior Technical Illustrator

Brian Washing
Technical Illustrator

Advertising Information

Janet L. Rocco, W1JLR
Business Services
860-594-0203 – Direct
800-243-7768 – ARRL
860-594-4285 – Fax

Circulation Department

Cathy Stepina
QEX Circulation

Offices

225 Main St., Newington, CT 06111-1400 USA
Telephone: 860-594-0200
Fax: 860-594-0259 (24-hour direct line)
Email: **qex@arrl.org**

Subscription rate for 6 print issues:

In the US: $29

US by First Class Mail: $40;

International and Canada by Airmail: $35

ARRL members receive the digital edition of *QEX* as a member benefit.

In order to ensure prompt delivery, we ask that you periodically check the address information on your mailing label. If you find any inaccuracies, please contact the Circulation Department immediately. Thank you for your assistance.

May/June 2022

About the Cover

Meredith Hillier, KG7EUM, and David Hillier, AA7XX, measure and report on the effects of metal obstructions on radio wave propagation. This complements a previous article by KG7EUM, "Effects of Common Building Materials on Radio Wave Propagation," which appeared in *QST*, January, 2022. In the present study, the authors investigate in more detail the effects of metal obstructions in both the far field and in the near field. They report on the resonance and phase effects of metal objects in the main beam of the Yagi antennas. A purpose-built radio test range includes elevated Yagi transmit and receive antennas 13.4 m apart, and a platform to hold the antenna array obstruction under test.

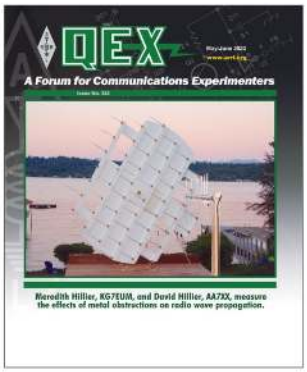

In This Issue

Index of Advertisers

The American Radio Relay League

The American Radio Relay League, Inc., is a noncommercial association of radio amateurs, organized for the promotion of interest in Amateur Radio communication and experimentation, for the establishment of networks to provide communications in the event of disasters or other emergencies, for the advancement of the radio art and of the public welfare, for the representation of the radio amateur in legislative matters, and for the maintenance of fraternalism and a high standard of conduct.

ARRL is an incorporated association without capital stock chartered under the laws of the state of Connecticut, and is an exempt organization under Section 501(c)(3) of the Internal Revenue Code of 1986. Its affairs are governed by a Board of Directors, whose voting members are elected every three years by the general membership. The officers are elected or appointed by the Directors. The League is noncommercial, and no one who could gain financially from the shaping of its affairs is eligible for membership on its Board.

"Of, by, and for the radio amateur," ARRL numbers within its ranks the vast majority of active amateurs in the nation and has a proud history of achievement as the standard-bearer in amateur affairs.

A *bona fide* interest in Amateur Radio is the only essential qualification of membership; an Amateur Radio license is not a prerequisite, although full voting membership is granted only to licensed amateurs in the US.

Membership inquiries and general correspondence should be addressed to the administrative headquarters:

ARRL
225 Main St.
Newington, CT 06111 USA
Telephone: 860-594-0200
FAX: 860-594-0259 (24-hour direct line)

Officers

President: Rick Roderick, K5UR
P.O. Box 1463, Little Rock, AR 72203

The purpose of *QEX* is to:

1) provide a medium for the exchange of ideas and information among Amateur Radio experimenters,

2) document advanced technical work in the Amateur Radio field, and

3) support efforts to advance the state of the Amateur Radio art.

All correspondence concerning *QEX* should be addressed to the American Radio Relay League, 225 Main St., Newington, CT 06111 USA. Envelopes containing manuscripts and letters for publication in *QEX* should be marked Editor, *QEX*.

Both theoretical and practical technical articles are welcomed. Manuscripts should be submitted in word-processor format, if possible. We can redraw any figures as long as their content is clear. Photos should be glossy, color or black-and-white prints of at least the size they are to appear in *QEX* or high-resolution digital images (300 dots per inch or higher at the printed size). Further information for authors can be found on the Web at **www.arrl.org/qex/** or by e-mail to **qex@arrl.org**.

Any opinions expressed in *QEX* are those of the authors, not necessarily those of the Editor or the League. While we strive to ensure all material is technically correct, authors are expected to defend their own assertions. Products mentioned are included for your information only; no endorsement is implied. Readers are cautioned to verify the availability of products before sending money to vendors.

Kazimierz "Kai" Siwiak, KE4PT

Perspectives

A Mentoring Experience

My introduction to Earth-Moon-Earth (EME) communications is an example of being on the receiving end of a mentoring exercise. At a ham meeting sponsored by the late Pete Rimmel, N8PR, at his home station, I remarked that my bucket list included working a station off the Moon. That was "a" station, as in one QSO would do it. Pete immediately consulted the moonrise tables and invited me back at a Moon-friendly time. So it began. Pete mentored me, then set me loose on his EME station. He did not warn me that I was an "initial," that is, a new call sign on 2 m EME. Pete grinned as multiple stations called me. With his guidance, my strategy was to start with the ones farthest east. Ukraine was first, then Poland, then more stations to the west before they lost the Moon on their western horizon. During that first session I worked 34 of them in less than three hours, exceeding my goal of "a" station!

In total I've worked over 100 EME stations, and even earned Worked All Continents on EME 2 m digital. With a top notch station like Pete's, and with his guidance, EME contacts with even rare ones like Mongolia are not out of reach. They are just a matter of patience and careful operating technique, based on a lot of planning, and skillful guidance by my mentor. Pete, N8PR, is now a silent key, but his mentorship did teach this old dog some new tricks.

In This Issue:

- Meredith Hillier, KG7EUM, and David Hillier, AA7XX, report the effects of metal obstructions on radio wave propagation.
- Mark Noe, KE1IU, accesses radio functions without the need for a PC.
- Jean-Claude Hénaux and Franck Daout describe the 'Gun' (Disk Yagi) antenna.
- Eric Nichols, KL7AJ, in his Essay Series, investigates reactance.
- Dr Sam Green, WØPCE, describes a versatile sweep generator measurement system.
- Hans Hartfuss, DL2MDQ, and Klaus Lohmann, DK7XL, estimate ionospheric drift velocity.
- Richard Grote, K6PBF, displays internet data in his Arduino based project.

Writing for *QEX*

Please continue to send in full-length *QEX* articles, or share a **Technical Note** of several hundred words in length plus a figure or two. *QEX* is edited by Kazimierz "Kai" Siwiak, KE4PT, (**ksiwiak@arrl.org**) and is published bimonthly. *QEX* is a forum for the free exchange of ideas among communications experimenters. All members can access digital editions of all four ARRL magazines: *QST*, *On the Air, QEX*, and *NCJ* as a member benefit. The *QEX printed edition* is available at an annual subscription rate (6 issues per year) for members and non-members, see **www.arrl.org/qex**.

Would you like to write for *QEX*? We pay $50 per published page for full articles and *QEX* Technical Notes. Get more information and an Author Guide at **www.arrl.org/qex-author-guide**. If you prefer postal mail, send a business-size self-addressed, stamped (US postage) envelope to: *QEX* Author Guide, c/o Maty Weinberg, ARRL, 225 Main St., Newington, CT 06111.

Very kindest regards,
Kazimierz "Kai" Siwiak, KE4PT
QEX Editor

Meredith W. Hillier, KG7EUM
4448 158th Ave. SE, Bellevue, WA 98006;
meredithwh13@gmail.com

David Hillier, AA7XX
4448 158th Ave. SE, Bellevue, WA 98006;
tc99mpertechnetate@gmail.com

Effect of Metal Obstructions on Radio Wave Propagation

The effects of metal obstructions in the far field and near field are reported.

Previously in M. W. Hillier, KG7EUM, "Effects of Common Building Materials on Radio Wave Propagation," *QST*, Jan., 2022, we tested the effects of various building materials on radio wave propagation. In this study, the effects of metal obstructions in the far field and in the near field are investigated in more detail. We looked at the resonance and phase effects of metal objects in the main beam. A radio test range (**Figure 1**) was built with elevated Yagi transmit and receive antennas and a platform to hold the antenna array obstruction under test. The transmit and receive antennas are 13.4 m apart.

We transmitted at 446.025 MHz using 2 W RF power from an ICOM 9100 transceiver. Transmit power was checked

Figure 1 — The radio wave propagation test range with KG7EUM at the spectrum analyzer.

with a Bird 4314C RF power meter. Measured SWR was about 1.2 for each antenna. Baseline measurements were obtained with a Rigol 1030A spectrum analyzer with everything but the obstruction set up and then again with the obstruction. Results are given as the difference between the two, in decibels (dB).

We want to understand the effects of metal objects, such as wiring or metal pipes inside the walls of a house, on radio propagation. A #12 AWG, half-wavelength long wire — which should be resonant — was placed in the main beam of the far field of both antennas. There was no measurable effect. Even with a single vertical wire up to 4.5 wavelengths long there was at most a 1 dB loss, depending on length. Therefore we constructed an array of linear conductors in the main beam, as shown in **Figure 1**. The array comprised 50 telescoping "FM radio" style antennas with adjustable length. These are isolated from ground.

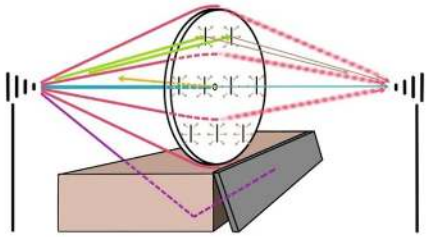

Figure 2 — Radio waves can be absorbed, or reflected, or diffracted around the obstruction. Signals that pass between the antennas in the array can also diffract. Diffraction underneath is largely blocked by an aluminum shield.

Effects of metal obstructions in the far field

Figure 2 shows various ways that a radio wave can interact with the obstructions and reach the receiving antenna. With large metal obstructions much of the signal will simply reflect. With long thin metallic obstructions (like wires and pipes), the interaction largely depends on whether the metal is oriented parallel with the polarization of the radio wave and whether it is of a length that is resonant. If it is resonant, it can interact strongly and reradiate the signal. The reradiated signal between the transmitting antenna and metal obstruction weakens with the inverse-square law and the reradiated signal from the metal obstruction also weakens with the inverse-square law. This reradiated signal can therefore be quite weak. This is the same phenomenon that occurs with radar. It is no wonder that there was no measurable effect with a single $\lambda/2$ wire in the far field of the main beam. However, there was a strong effect with an array of 50 antenna obstructions in the far field. The received signal is a combination from the various signals shown in **Figure 2**, including the direct ray, diffraction, and reradiated signal. These arrive with various phase relationships, depending primarily on the relative distances travelled.

As we might guess based on our experience with antennas, the effect of a linear metal obstruction depends on its length and resonance effects. The effect of varying the length of the vertical antennas

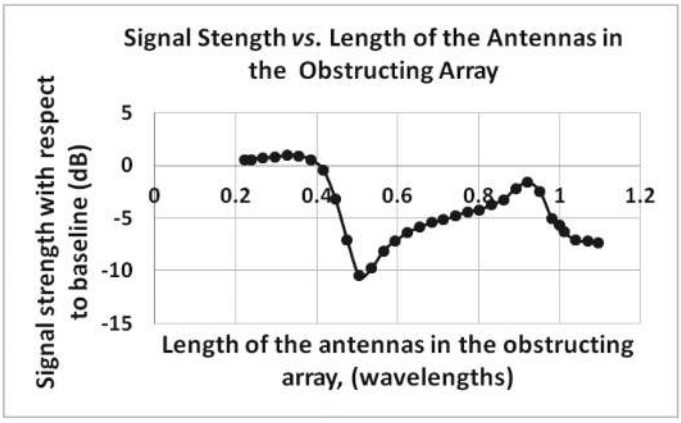

(A)

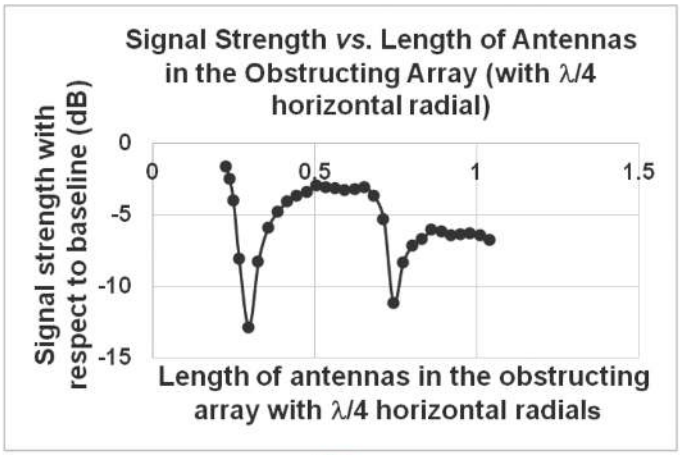

(B)

(C)

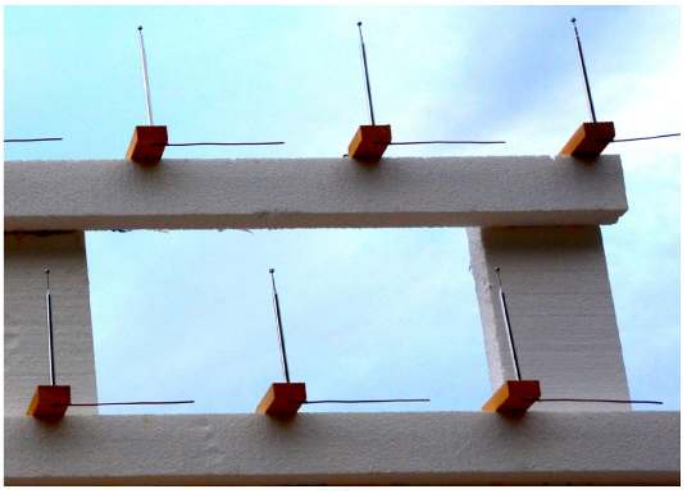

(D)

Figure 3 — Magnitude of obstructing effect *vs.* length of antennas in the 50-antenna obstructing array for vertical antennas without radials (A) and (C), and for antennas with quarter-wavelength radials (B) and (D). Note the strong obstructing effect related to resonance.

in the obstructing array was tested. The experiment was repeated after attaching λ/4 radials (#12 AWG horizontal bare copper wires attached to the base of the vertical antennas). The lengths of the 50 vertical antennas in the array were adjusted from just under a quarter to just over one wavelength at the test frequency in 2 cm increments. There is a very strong dependence on length, as shown in **Figure 3**. The antenna array obstruction causes a strong drop in signal strength at resonance, when the vertical antennas (without radials) are half a wavelength long and when the vertical antennas with radials are λ/4 long. In both cases, resonance should occur again for every λ/2 increase in length: λ/2, λ, 3λ/2…, for the antennas without radials, and λ/4, 3λ/4, 5λ/4…, for the antennas with λ/4 radials. These effects are seen in **Figure 3**, although the pattern becomes less clear as antenna length increases beyond about 3λ/4, probably due to interaction between antennas in adjacent rows on the array as the antennas start to overlap. The blocking effect is much weaker at non-resonant lengths. Figure 26A in the 24th edition of the *ARRL Antenna Book* discusses this effect, as it applies to guy wire lengths.

A signal strength azimuth plot is shown in **Figure 4A** for the Yagi transmit antenna without and then with obstructions in the far field. **Figure 4B** shows the author holding the Yagi for one of the no-obstruction tests. There is a 5.9 dB loss in the forward direction with an array with 50 resonant λ/2 antennas and a 12.8 dB loss with a solid 8 by 8-foot aluminum foil reflector. Note the strong reflection in the reverse direction with a signal approximately 13 dB stronger at 180° with either obstruction than without. In fact the signal in the reverse direction with the reflecting obstructions is only about 7.5 dB weaker than the signal in the forward direction with no obstruction. Note that the array with a such a large number of closely-spaced antennas (with 0.42 λ horizontal spacing and 0.5 λ vertical spacing) behaves similarly to a solid reflector. We are familiar with this concept in that a parabolic dish with close mesh spacing, relative to wavelength, behaves as a solid reflector.

Linear metal obstructions are commonly vertical or horizontal but can be at any orientation. The effect of the antenna array on the vertically-polarized radio waves being tested depended strongly on angle with respect to vertical, as shown in **Figures 5A** and **5B**. There is a strong effect when the array antennas are vertical and no effect when the array is horizontal. The array is essentially "invisible" when horizontal (cross-polarized). This is not surprising since we know that a horizontally-polarized antenna will reject a vertically-polarized radio wave very strongly. Interestingly, one can make use of the array to essentially "reorient" the radio wave to match a vertically-polarized radio wave to a horizontally-oriented receiving antenna.

By placing the 50-antenna array with resonant-length antennas at 45°, the array will still intercept the vertically-polarized wave, but with a theoretical loss of 3 dB.

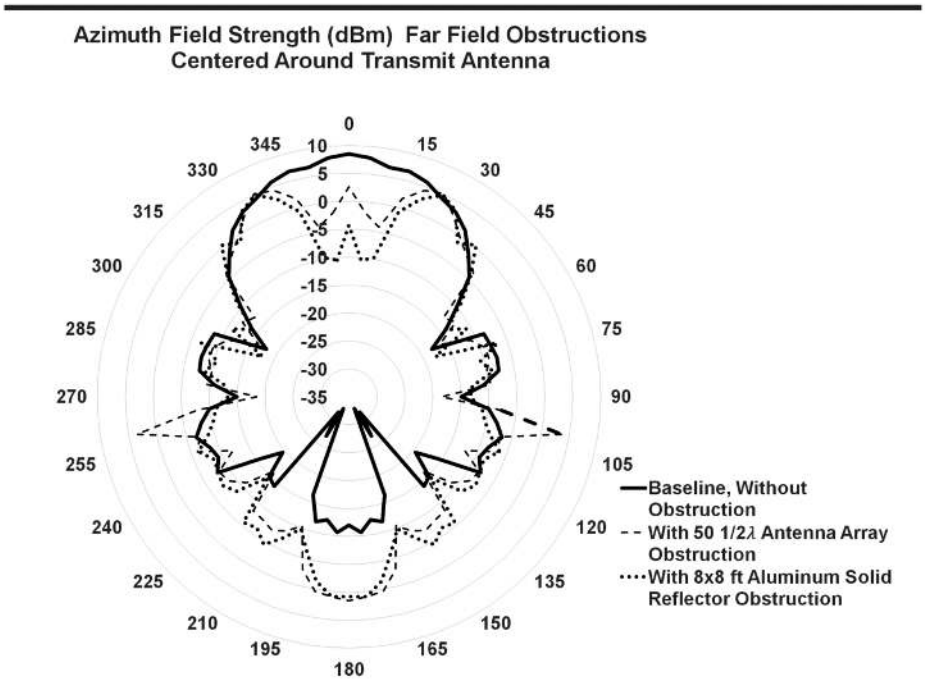

(A)

(B)

Figure 4 — Field strength azimuth plot (A) for the Yagi transmit antenna without obstructions (solid) and with obstructions consisting of an array of 50 resonant λ/2 antennas (dashed) and an 8 by 8-foot aluminum foil reflector (dotted) in the far field. 180° of data were collected and then mirrored to create the 360° plot. In (B) the author is shown holding the Yagi for a no-obstruction test.

The signal power should be $[\sin(45°)]^2$ = 0.5, or –3 dB, compared to that with vertical orientation. The reradiated signal at 45° will be received with a horizontal antenna with another 3 dB loss. There would therefore be a 6 dB loss with an efficient array — as long as there is not a significant double inverse-square law effect. This is much less than the loss due to cross-polarization expected without the array, which can exceed 20 dB. In my tests, there was an 18.1 dB loss between the vertically-polarized transmitting antenna and a horizontally-oriented receiving antenna compared to both oriented vertically with no array in between. With the array, at 45°, there was only a 7.2 dB loss, close to the theoretical. This same effect is seen with light polarizer filters. Placing a horizontal polarizer in front of a vertical polarizer results in no light transmission, while placing an oblique filter in between allows light transmission.

In summary, a single linear metal object in the far field has a negligible effect on radio wave propagation, due to diffraction around the obstruction and due to the double inverse-square law effect of the retransmitted signal. A large metal reflector or multiple linear metal objects of resonant length, and of the same polarization as the incident radio wave, resulted in strong attenuation. For ungrounded linear obstructions, the greatest effect is seen with lengths of a multiple of λ/2. While not tested here, resonance for grounded linear metal obstructions would occur at a λ/4 length and then at λ/2 intervals thereafter. With an 8 by 8-foot aluminum reflector, signal strength dropped 12.8 dB, and with a 50-antenna array of λ/2 length antennas, signal strength dropped 5.9 dB.

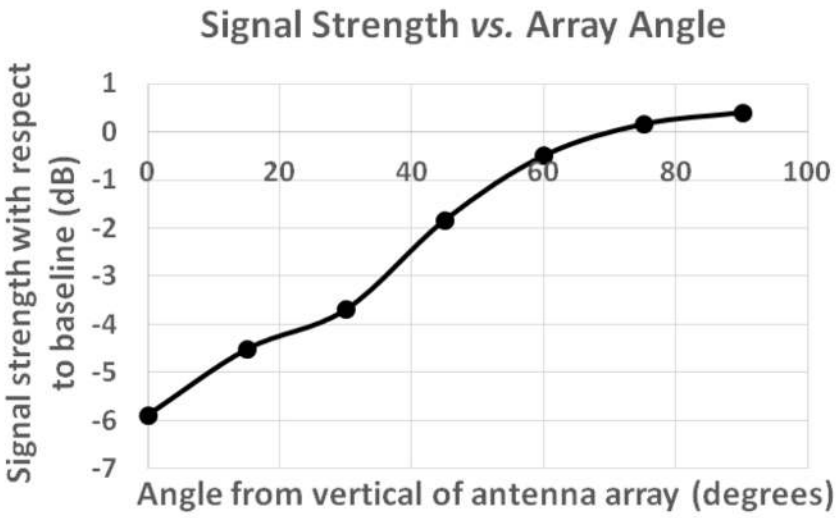

(A)

(B)

Figure 5 — Effect of angle of a 50-antenna obstructing array on vertically-polarized radio waves. (A) The strongest attenuation occurs when the array of antennas is vertical (0°), and there is no significant effect when horizontal (90°). (B) shows the 50-antenna array at a 60° angle from the vertical.

Effects of metal obstructions in the near field

In this section the effects of wire length and orientation of a wire obstruction in the near field of a transmit antenna main beam are reported. Experiments with a metal wire placed in the near field of the transmit antenna, revealed a relatively strong effect on received signal strength, unlike with a single wire obstruction in the far field. In the near field, capacitive or inductive coupling can occur between the obstruction and the transmitting antenna. A more profound impact might be anticipated than when the obstruction is in the far field — where the obstruction is in the radio wave beam but not directly coupled with the antenna.

A radio test range, **Figures 6A** and **6B**, was configured with elevated Yagi transmit and receive antennas 13.4 m apart, and with no obstructions between the antennas. Then, a single #12 AWG solid copper wire was placed just in front of the transmit antenna using a thin wooden rod attached to the boom of the antenna to hold the obstructing wire. Its length and orientation were varied.

Unlike when a single wire obstruction was placed in the far field, there was a strong effect on signal strength by a single vertical wire in the near field. As seen in **Figure 7**, this effect was strongest for a vertical λ/2 wire obstruction, ranging from a loss of 1.2 dB to 3.6 dB, depending on distance in front of the antenna. While this is significant, it would not necessarily disrupt a radio communication. SWR was tested for the λ/2 length wires at the various distances from the antenna; SWR remained in an acceptable ranging between 1.1 and 1.9, except at λ/4 in front of the antenna where SWR was 2.2. A horizontal wire of λ/2 length was also tested at the various distances, revealing no effect.

It is the overall length of the wire that determines if the wire is resonant, and will strongly interact. In **Figure 8A** we see

this effect with a 90° bent wire (pictured in **Figure 8B**) in the near field with a λ/2 vertical component and a variable horizontal "radial" component extending to the right.

Figure 9 shows the azimuth field strength pattern when a λ/2 resonant #12 AWG copper wire was placed in front of the transmitting antenna within the near field. There is a 2.5 dB drop in the forward direction, compared to no-obstruction baseline. This is a significant drop, but perhaps not as substantial as one might have expected. What is perhaps more interesting is the effect in the reverse direction (at 180°), where there is a 9.7 dB signal increase. One can think of the wire as redirecting the energy from the forward direction to the reverse and side directions. If one needed to redirect a signal in the reverse direction or to the sides with a fixed directional antenna (that cannot easily be rotated) by placing a large reflector or simply a λ/2 wire in front the antenna. This would not be the usual recommended approach and its effects would be somewhat difficult to predict without careful analysis, but in a pinch it could be worth a try to communicate with someone in the reverse or side directions.

To this point, the effects of a resonant length wire in front of the directional transmitting antenna have been studied. What happens if a λ/2 wire is placed near the driven element of the Yagi transmitting antenna from the side? Interestingly the wire had very little effect on the SWR or the signal strength at most distances. At λ/8

(A) (B)

Figure 6 — (A) shows a #12 AWG vertically-oriented wire obstruction mounted to a wooden rod attached to the boom of a Yagi transmit antenna. The receive antenna is 13.4 m away, seen to the left in the distance. (B) shows a horizontal wire obstruction.

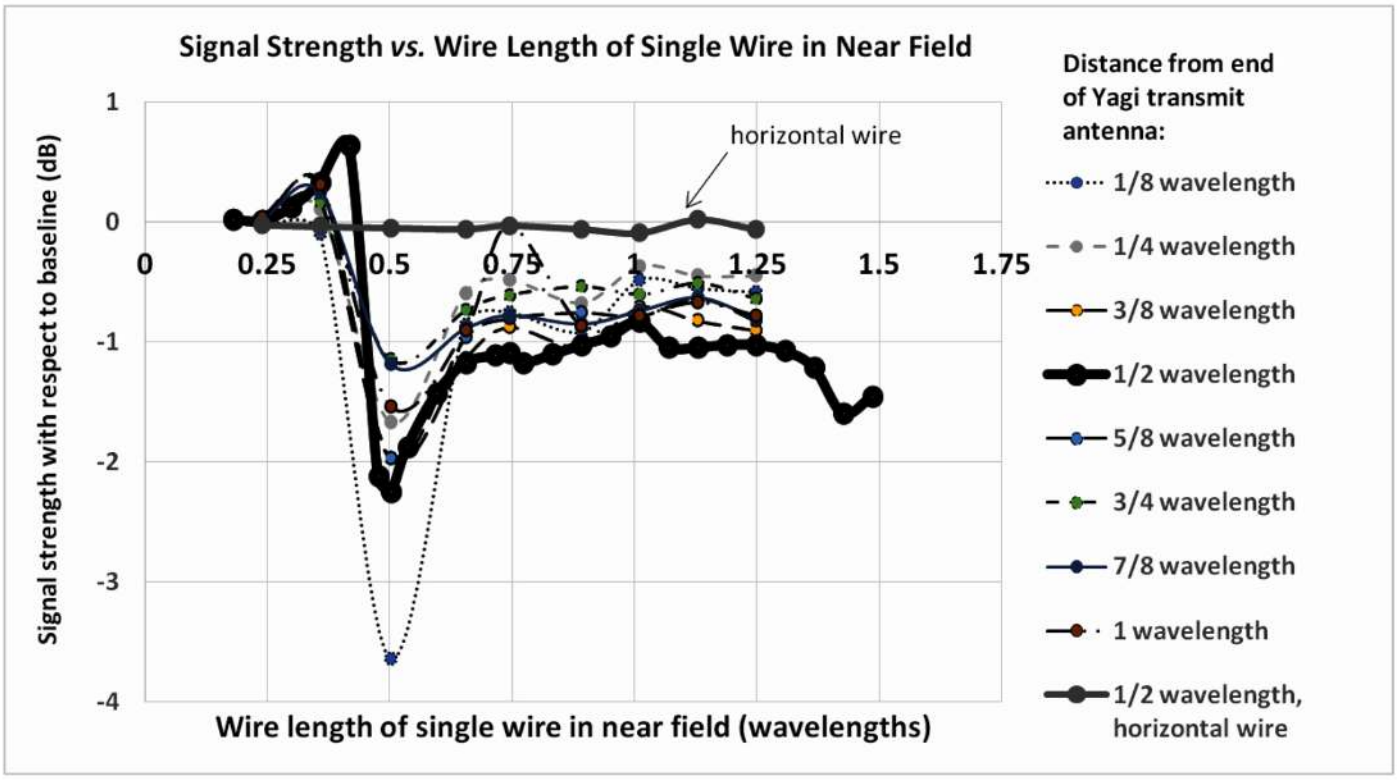

Figure 7 — Effect of a #12 AWG obstruction placed in front of a vertically-polarized Yagi transmit antenna. The result for a horizontally oriented wire placed λ/2 in front of the last director element of the Yagi transmit antenna is also shown. The horizontal wire has no effect.

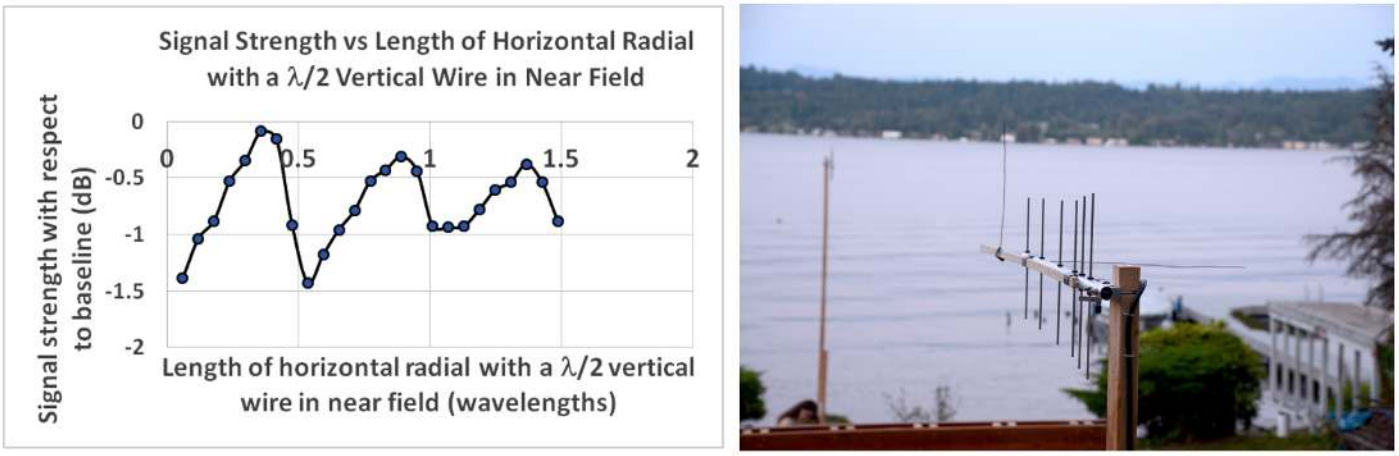

(A) (B)

Figure 8 — (A) Signal strength for a vertical λ/2 long #12 AWG copper wire placed in the near field λ/2 in front of the transmit antenna, with a (B) variable length horizontal "radial" attached to the obstruction and extending horizontally to the right.

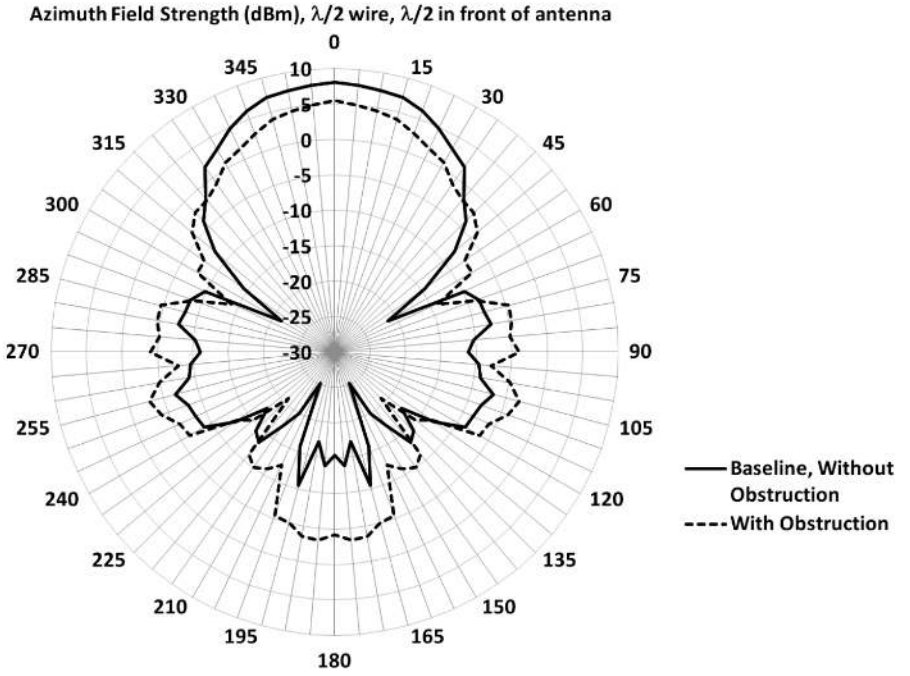

Figure 9 — Azimuth field strength pattern for a single #12 AWG copper vertical wire of λ/2 length placed directly in front of the Yagi transmit antenna in the near field, λ/2 in front of the last director element. Data was collected for 180° and then mirrored to create the 360° plot.

distance (8 cm in the 70 cm band) the SWR was 1.15, and signal strength dropped 0.36 dB, an insignificant change. When it was placed very close, at 1 cm distance, the SWR was very poor, at 5.2, and the signal strength dropped 6 dB.

In summary, linear metal obstructions in the near field can have a substantial effect. This was not true in earlier experiments with a single wire obstruction in the far field of both the transmit and receive antennas. A λ/2 length linear obstruction, placed λ/2 in front of the transmit antenna (well within the near field) of the same polarization, resulted in a 2.5 dB drop. While significant, this is not a huge drop. The effect is strongly dependent on the length of the wire obstruction. It is strong for a resonant length of λ/2 and much weaker for other non-resonant lengths. If there is a perpendicular radial attached to the base of the wire, it is the total length that determines resonance. Resonance occurs at a wire length of λ/2 and multiples thereof, for obstructions not connected to ground. Although not studied here, resonance would occur at a length of λ/4 for grounded linear metal obstructions and for multiples of λ/2 added to that length.

[All photos by David Hillier, AA7XX.]

Meredith Hillier, KG7EUM, a senior at Newport High School in Bellevue, Washington, earned her Technician Class license at age 9 and her General Class license a year later. She is an active member of the West Seattle Amateur Radio Club, and was selected in both 2019 and 2020 for the International Science and Engineering Fair. In February, 2020, Meredith was inducted as a Lifetime Fellow into the American Junior Academy of Sciences.

David Hillier, AA7XX, has been fascinated with radio since age 10 and finally got his Amateur Extra class license at age 52. David has a PhD in electrical engineering. Evenings, he enjoys ham radio. He is a member of the West Seattle Amateur Radio Club. David especially enjoys teaching new students and sharing his enthusiasm about ham radio.

Mark Noe, KE1IU

23 Harvest Glen, East Lyme, CT 06333; **ke1iu@arrl.net**

An Arduino Based Dial Box for Extending the Control Panel of Modern Transceivers

Conveniently extends access to radio functions without the need for a PC.

Modern transceivers are packed with useful features that improve the quality of received signals, tailor the properties of transmitted signals and enhance ergonomics. These radios often come with rich front-panel displays and touch screens that enable exploring functions far beyond what is offered on the front panel controls. While most commercial transceivers are well designed with operator ergonomics in mind, sometimes frequently used functions are buried in sub-menus that make them difficult to access. This situation is inconvenient if repeated adjustments are needed. Most of today's transceivers can connect to a PC, enabling control of their functions through software. While computer control is an attractive solution to this problem, it requires the user to have a PC attached to the radio, which may not be practical for field-based operation. Furthermore, having the radio dashboard open on the computer may not be convenient if windows are also open for logging or digital communication software.

I have several Icom radios, each of which has several functions that can be accessed only in sub-menus. For example, the RF power adjustment, notch adjustment and microphone gain adjustments for my Icom 7610 require accessing a sub-menu function and then turning an omni-control to change these settings. While these settings are infrequently adjusted by many users, I change the RF power setting often, depending on whether I am using my linear amplifier (which accepts a maximum 40 W of drive) or operating barefoot. I wanted a device that would bring the RF power control to the front panel of a console so that I could easily change that setting. Moreover, since the RF power setting is not always visible on the Icom display, I wanted to see the status of the RF power setting regardless of whether I adjusted it at the radio or at the off-board console. Therefore, the ideal device would also incorporate a display. Finally, I wanted the device to be configurable for use with other transceivers and capable of operation without an attached PC, which would be ideal for portable operation. After considering several possible solutions, I was inspired by a publication of an Arduino-based dial box for use with software defined radios [1]. The device described here improves on that design by incorporating a color TFT display to indicate the value of settings regardless of whether they are changed at the radio or on the dial box. It uses rotary encoders to allow independent control of each setting at either location and incorporates additional buttons and dials for

Figure 1 — Front panel view of the controller.

control of up to 12 different functions that are defined by the user.

Hardware Design

The controller is designed around an Arduino Due computer, although an Arduino Mega can likely be used in its place. A smaller Arduino, such as the Uno, will likely not work because of the program size, and their limited number of digital I/O pins. The Due offers several features which, while not used here, represent opportunities to add to the design. For example, the Due offers an additional USB port, which could be used to send output to a PC if desired. Also, it has additional interrupt pins that could increase responsiveness with digital encoders or enable the use of other I/O devices. My implementation did not require coding interrupts to enable smooth and seamless control response. It also may be possible for the secondary USB port on the Due to connect directly to a USB port on the radio, although that option was not explored.

My system, **Figure 1**, was designed for use with Icom transceivers through their CIV port. This port is a one-wire serial-based communication system that connects to other peripherals on a common bus. In order to enable communication with the Arduino Due, a level converter is needed to deliver CMOS 3.3 V logic at the Arduino side from TTL 5 V logic coming from the transceiver CIV port [2]. Level conversion is accomplished through Q1 and Q2, which connect to the TX pin and RX pin of one of the hardware serial ports on the Due, see **Figure 2**. The gates of these MOSFETs are connected to the 3.3 V line of the Arduino. The Arduino (U2) digital pins D18 and D19 (serial TX and RX, respectively) are

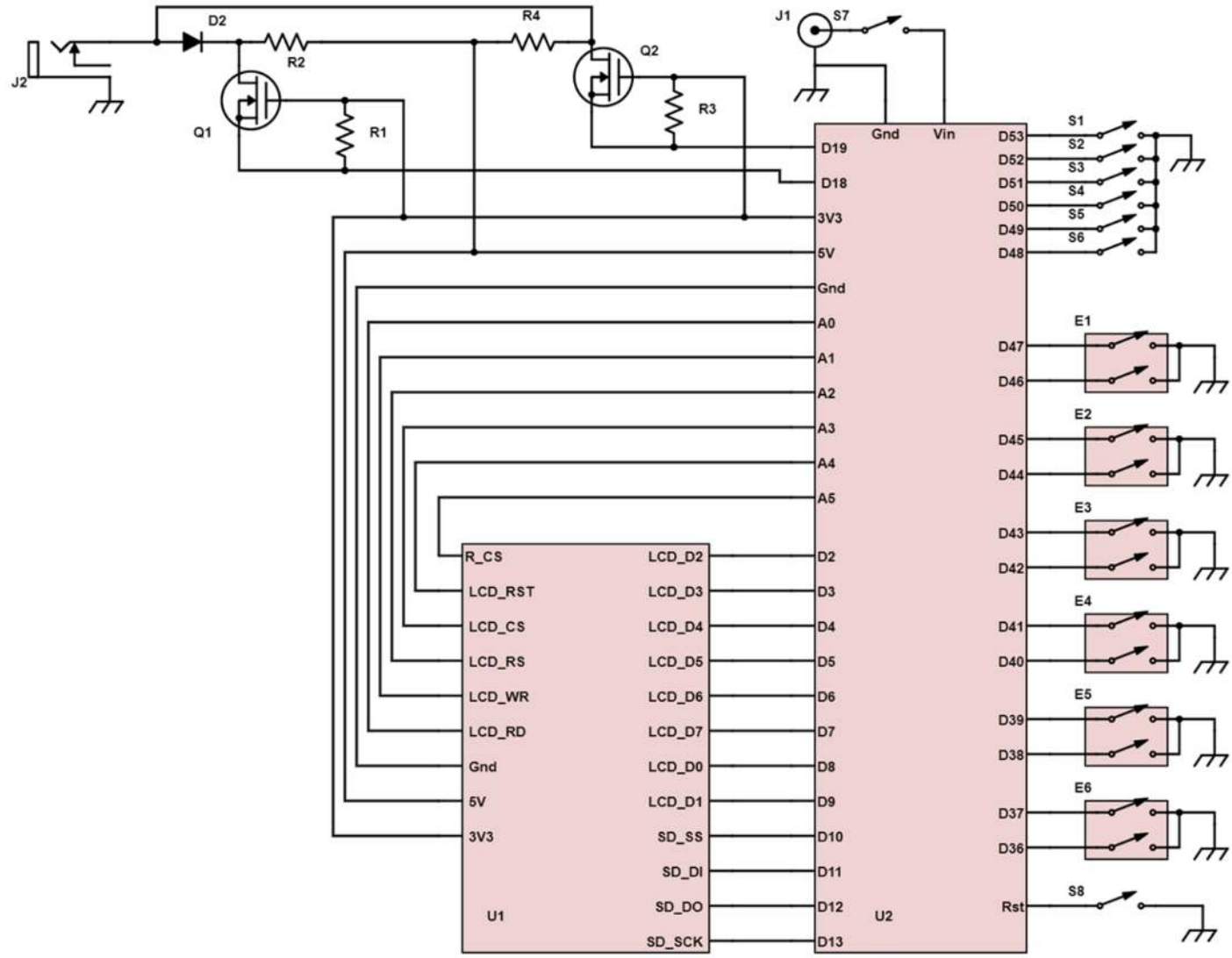

Figure 2 — Schematic diagram of the controller for Icom radios. Components list:

D2 — 1N4148 switching diode
E1-E6 — Incremental rotary encoder (Digi-Key PEC11R-4220K-S0024-ND)
J1 — 5.5 mm x 2.1 mm coaxial power jack (Amazon.com)
J2 — 1/8 inch mono or stereo phone jack
Q1-Q2 — 2N7000 MOSFET
R1-R4 — 10 kΩ 1/4 W resistor
S1-S6 — SPST tactile pushbutton switch
S7 — SPST toggle switch
S8 — SPST tactile pushbutton switch – or use one of the switches on the rotary encoders.
U1 — 3.5 inch touch screen Kuman Model 8541612321 (Amazon.com)
U2 — Arduino Due microcomputer.

pulled high by R1 and R3. The drains of Q1 and Q2 are pulled up to 5 V by R2 and R4. When high bits are received from the CIV port, the MOSFET is tied high (**off**), and the RX pin on the Arduino (D19) is high. When low bits are received from the CIV port, the drain of Q2 is pulled low, which causes the MOSFET substrate diode to conduct, causing the RX pin D19 on the Arduino to be pulled low. Likewise, when low bits are transmitted from the Arduino TX pin D18, the MOSFET source pin is grounded, which turns the MOSFET **on**, leading to the drain of Q1 being pulled low. This situation causes D2 to conduct, producing a digital low at the CIV port. This circuit therefore enables both level conversion and the adaptation of one-wire communication required by the Icom transceiver to 2-wire serial communication required by the Arduino **[3]**. If you decide to use an Arduino Mega with this project, you will not need level conversion, as the Mega operates at 5 V logic. You will, however, still need to convert one-wire serial to 2-wire communication for Icom radios.

Kenwood and Yaesu radios have RS-232 or USB ports directly accessible on their rear panels. Interfacing to these transceivers is more straightforward. Any RS-232 to TTL adaptor can be used (such as the Anmbest MAX3232 converter available on Amazon; this converter offers level conversion to 5 V or 3.3 V TTL logic). Modify the circuit shown in **Figure 2** to omit Q1, Q2 and their associated components, and connect the module directly to the Arduino. The TX and RX pins on the board should connect to pins D19 (RX) and D18 (TX), respectively. The Vcc pin should be connected to the 3V3 pin on the Arduino (for the Due) or the 5 V pin (for the Mega 2560), and the Gnd pin should be connected to ground. This project was tested on a Kenwood TS480SAT transceiver but was not built or tested for Yaesu radios. This Kenwood transceiver uses hardware flow control, so the CTS pin on the Anmbest converter was connected to Vcc. Also, I required a null modem between the transceiver and the Anmbest converter to get valid serial communication to the transceiver. You should check the instructions that come with your interface for proper wiring directions. Some experimentation may be required depending on your transceiver.

My controls consist of six tactile pushbutton switches connected between a digital input pin and ground. I used six rotary encoders for the dial controls. Each requires two digital pins from the Arduino. Because the rotary encoders also incorporate a momentary pushbutton switch, they can be wired to six additional digital input pins to give more pushbutton controls if desired. I used one of these switches to enable resetting the Arduino (S8 in the schematic), although a separate pushbutton switch could be used for that purpose if desired.

I used a Kuman 3.5 inch TFT display that even includes a touch-screen feature and an SD-card for storing high resolution images. I did not employ these features in this design, but it offers yet another opportunity for expansion if desired. Since the display uses 18 I/O pins on the Arduino, only the larger Arduino computers are suitable for this project.

My unit is housed in an aluminum console box (Digi-Key HM3092-ND). I mounted the TFT display underneath the front panel such that it was completely recessed behind the opening and was held in place with screws set into strips of wood glued to the back of the panel. I placed a piece of glass into the recessed opening to create a flush surface on the front panel, and I used black caulk to fill in the gap between the glass and the aluminum surface. Of course, this mounting arrangement will not work if you intend to use touch-screen features of the display. All connections were made using DuPont connectors and ribbon cable.

Software Design

Custom Arduino libraries were created for this project and are well commented to enable modification for different radios **[4]**. In addition, the Supplementary Material in the **www.arrl.org/QEXfiles** web page for this article contains detailed descriptions of how these libraries work so you can modify them if needed. Icom transceivers have fundamental differences in their CAT communication protocol relative to Kenwood and Yaesu. Each will be described briefly below.

Icom radio command structure

Icom radios use binary serial communication with a byte structure shown in **Figure 3**. Each command from the controller to the radio begins with a preamble (two FE bytes), followed by the transceiver CIV address (in hexadecimal) and the controller address (set to E0 in this case). This command structure allows several transceivers and accessories to be connected together on the same CIV bus. The next piece of data is the command number for the desired command to send or interrogate (**Cmd**), followed by the subcommand (**Scmd**). These data are both sent as hexadecimal bytes, and the CIV reference manual for your radio can be used to identify the appropriate parameters for the functions you wish to control. After these values are sent, the actual data for the control setting is sent as a BCD (Binary Coded Decimal) value. Finally, the byte FD ends the message. The command structure is identical for received data from the radio, except the transceiver CIV address is sent after the controller address. When reading data from the transceiver, the code parses each byte string to identify the header, the command and subcommand, and then the appropriate bytes for the data. The data value is then sent back to the main program for rendering on the display.

Yaesu and Kenwood command structure

Yaesu and Kenwood transceivers use

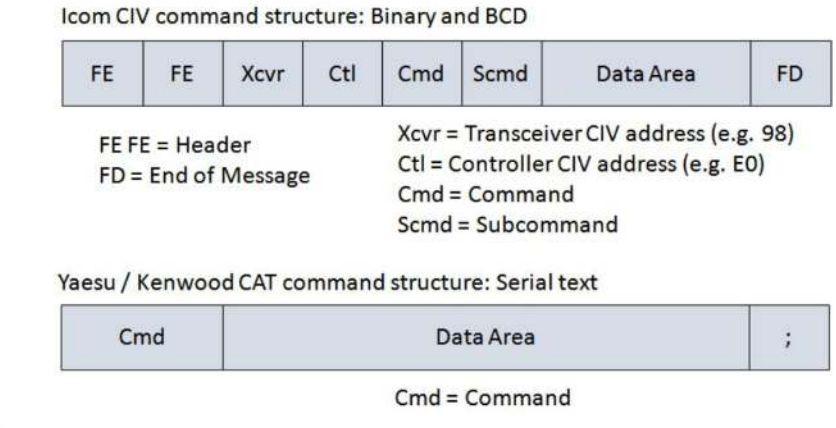

Figure 3 — Command structure for Icom and Yaesu/Kenwood computer control.

character-based serial communication (**Figure 3**), and only one radio can be connected to each COM port on the computer. The use of a dedicated COM port simplifies the communication protocol, which begins with a two-letter text command and is followed by the numerical representation of data to adjust that function. All commands end with a semicolon terminator. As such, pointers to character arrays are passed to the objects and functions in the software to enable sending the appropriate command text string via the serial port. Likewise, characters coming in on the serial port are compared with character arrays defined for each button or dial to define a match, at which point the data is read as a set of ASCII characters and is then converted to an integer for processing and display.

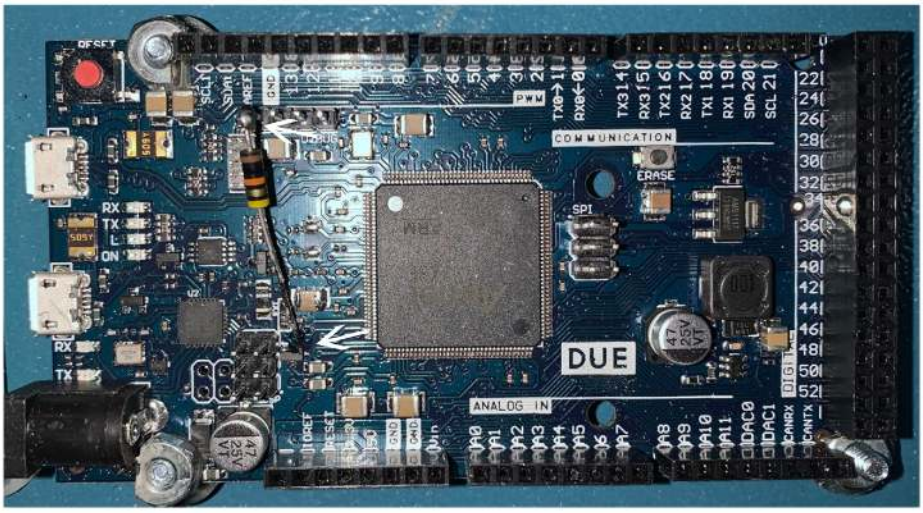

Figure 4 — Modification of the Arduino Due to prevent hard reset. Insert a 10 kΩ resistor between the left-most pin on the Debug Header and the right-most pin on the surface-mount transistor.

The main program

The main program uses one of these custom libraries as well as the *Adafruit_GFX.h* library and the *MCUFRIEND_kbv.h* library to drive the TFT display. The software works by checking first for any change in status of the console controls using the **updatebuttons** function. If a button is pressed or a knob is turned, the Arduino changes the value stored in memory for the prior state of that control and then sends the data as a binary string to the transceiver (for Icom) or a text string (for Yaesu or Kenwood). The TFT display is updated accordingly through the **updatedisplay** function. Next, the Arduino looks for incoming data from the radio using the **icomchange** or **yaesuchange/kenwoodchange** function. Should any of the console controls be updated from the radio itself, this function updates the display, and the current value of that control is stored in memory. Thus, the radio and the console offer completely independent control of the transceiver.

Customizing for Your Radio

You must download the libraries and the main code from the **QEXfiles** web page. Place the library folders contained therein (*DialBoxIcom*, *DialBoxYaesu*, *Adafruit_GFX*, *MCUFRIEND_kbv* and *RotaryEncoder-master*) into your **/Documents/Arduino/Libraries** folder. Note that the *DialBoxYaesu* library is also intended for Kenwood radios, as they both use similar CAT command structures and serial communication protocols. Three versions of the code are included in the Supplementary Material on **QEXfiles**. Versions titled "*DialBoxIcomGeneric, DialBoxKenwoodGeneric* or *DialBoxYaesuGeneric* will be the simplest places to start. Specific tested implementations can be found in the programs *DialBoxIcomKE1IUVersion* and *DialBoxKenwoodExample*. Place the appropriate folder file in your **/Documents/Arduino** folder and double click on the *.ino* file contained inside of it.

The controller can be scaled to add any number of pushbutton switches or rotary encoders, limited only by the number of pins on the Arduino. In the main program, one adds or subtracts button or dial objects accordingly. Each object is defined by its hardware pin number, commands that the radio expects when that control is adjusted and parameters defining the data characteristics for that control. A more detailed description of how the program works and how to modify the code for your custom controller appears in the supplementary material on **QEXfiles**.

Modifying the Arduino Due

Some versions of the Arduino Due are known to have a problem on startup, wherein a hard reset is applied to the board, and the internal flash memory that stores the program is erased. This problem results in an all-white blank display. When this happens, the program must be uploaded to the board again, which is inconvenient. My Due clone has this issue, and it is easily corrected by attaching a 10 kΩ resistor between the gate of Q3 and the first pin of the Debug Header as shown in **Figure 4**. This issue is well documented on the internet (search for Arduino Due reset problem) **[5]**.

Testing and Operation

It is a good idea to ensure that the level converter is working properly and outputs the correct signal voltage for your radio. For the Icom version, this test can be done with an oscilloscope connected to the one-wire serial output on the controller. Check to see that TTL logic (5 V) is present and that binary 0s are sent when adjusting the controls. For the Yaesu version, the oscilloscope can be connected to the TX pin of the RS-232 port of the controller. Alternatively, you may be able to connect a computer to the controller serial port and monitor the control codes being sent as text when buttons or knobs are pressed — note that you may need to use a null modem for this purpose; also the console does not offer flow control. After this testing is complete, connect the controller to your transceiver and apply power to the console. This operation should yield a blue display that populates with values within 5 seconds. If it does not, check that the serial communication parameters (CIV address and baud rate for Icom radios, or port configuration and baud rate for Yaesu/Kenwood radios) are set appropriately. If the display is white, try resetting the Arduino board by depressing the reset button on the Arduino board or on your control panel. If that does not work, it is likely that there is a bad connection to one of the digital pins of the TFT display or the wiring to the display is incorrect.

If the display is blue but is not updating from the transceiver, check to see if adjusting the console buttons or dials causes their parameters to appear on the display. If so, then the likely problem is a communication issue with the radio. Check to see if adjusting the controls on the console yields any response on the transceiver. If not, you will need to assess whether the Arduino is sending the appropriate binary (for Icom) or textual (for Kenwood or Yaesu) serial commands. This test can be done by un-commenting the *#define DEBUG* line in the *.cpp* library file, connecting a PC to the USB port and monitoring communications using a terminal program capable of displaying binary values. For Icom radios, *Realterm* is a good freeware application for that purpose. Check to see that the binary strings sent after adjusting one of the controls correspond to what the radio is expecting. If not, you will either need to modify the *DialBox* library or evaluate whether there is an error in setting the characters/bytes for each control you defined in the main program. Identifying problems with the controller's ability to send commands to the radio will usually identify corresponding issues that are preventing the display from updating. Remember to comment out the *#define DEBUG* line in the *.cpp* library file when you are finished, and upload the program again into the Arduino.

All parts for this controller can be obtained from Amazon and Digi-Key for under $100 if everything is purchased new. The controller operates with nearly instantaneous response to inputs on the console, and inputs from the radio are received within 5 seconds. Because the controller uses rotary encoders for the dials, any setting changes on the radio are incremental to the last setting on the controller and vice versa. Finally, the console can be scaled to whatever number of controls you would like to have on the panel. Because the console operates without the need for an attached PC, it is a handy tool for expanding the number of controls on your transceiver front panel whether in the home station or the field.

[Images by the author.]

Mark Noe, KE1IU, was first licensed in 1980 as a Novice, KA2KPB, at age 10. He currently holds an Amateur Extra class license and has been a member of the ARRL for 42 years. Mark leads a drug discovery research group in the pharmaceutical industry. He received his Bachelor degree in chemistry from the University of Michigan and his PhD in organic chemistry from Harvard University. He enjoys building antennas and station accessories. Mark operates SSB, CW, RTTY and FM modes. He occasionally operates the low earth orbit satellites and enjoys HF DXing. You can reach him at ***ke1iu@arrl.net*** *or* ***ke1iumark@gmail.com****.*

Notes

[1] M. Stott, "An Arduino Based Knob Box," *ARRL Handbook for the Radio Amateur, 2019, Station Accessories and Projects*, p. 33.

[2] For more information on the level converter circuit, see **https://www.hobbytronics.co.uk/mosfet-voltage-level-converter**.

[3] For more information on level shifting circuits, see **https://hackaday.com/2016/12/05/taking-it-to-another-level-making-3-3v-and-5v-logic-communicate-with-level-shifters/**. The section on bidirectional level shifters inspired the circuit shown here.

[4] The Icom library was partially inspired by code from a transverter controller project described at, **https://www.qsl.net/on7eq/projects/arduino_icom_ci-v_proxy.htm**.

[5] For more information on the Due reset problem see, **https://copperhilltech.com/blog/arduino-due-design-flaw-due-wont-start-after-poweroffon-requires-reset/**

Jean-Claude Hénaux
39 Avenue du Général de Gaulle, 17730 Port des Barques, France;
jeanclaude.henaux@free.fr

Franck Daout
34 Rue Roque de Fillol, 92810 Puteaux, France;
fdaout@parisnanterre.fr

Build Your Own 'Gun' (Disk Yagi) Antenna

This high directivity antenna has moderate bandwidth and is easy to build.

We propose to rediscover and build an antenna that is particularly well suited for use in the 1 to 4 GHz frequency range, see **Figure 1**. The 'Gun' (or Disk Yagi) antenna belongs to the end-fire antenna family. It is easy to build and does not need a balun. For the same directivity, it is less bulky than a horn antenna. The relative bandwidth, B, for an SWR of 2 is about 5% to 7%. In the following, we will see how its geometry determines its radiation pattern. The Gun antenna dimensions must be chosen according to the frequency of use and the desired directivity. We provide a computer program to calculate all dimensions of the antenna according to these objectives. Some construction advice is given and a realization is presented.

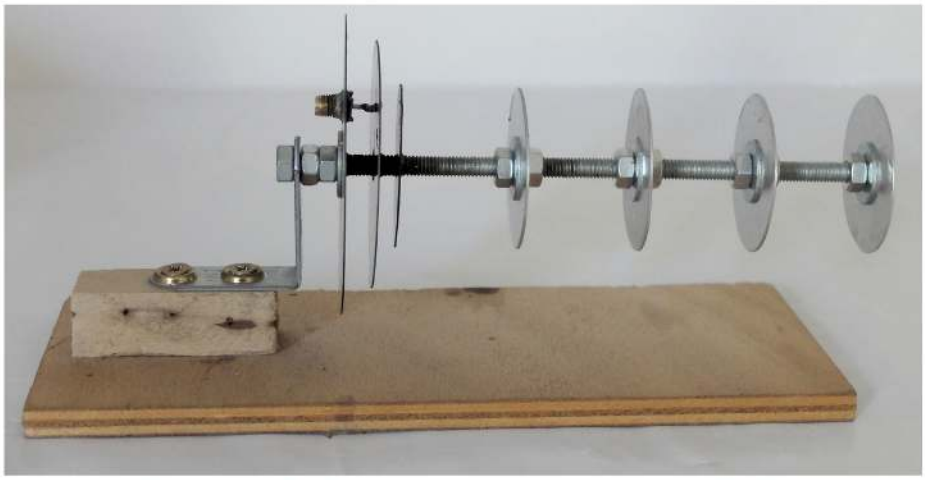

Figure 1 — A Gun (Disc Yagi) antenna for operation at 2,450 MHz.

End-fire antennas use surface waves

These antennas essentially consist of a moderately directional transmitter and a surface waveguide (SWG) that propagates a wave with a speed v_m that is less than the speed of light c. The role of the SWG is to sharpen the radiation pattern.

The complete analytical calculation of an end-fire antenna is not feasible, and a more qualitative and experimental approach was initially required. Since the first papers on the subject were published, powerful tools are now available. On the one hand for synthesis we use numerical simulation (*NEC*, *HFSS*, *CST*, etc.), and on the other hand for measurement we use Vector Network Analyzers. These tools allow us to compare precisely the predictions and the measurements, and bring the realization of the projects.

What is in a Gun antenna?

This antenna resembles a Yagi antenna whose dipoles have been replaced by metal disks. The following work was inspired by the achievements of Alexander Kryukov, alias "Kreosan," see YouTube [1]. **Figure 1** shows an end-fire antenna for the reception of 2,450 MHz transmissions. The two disks on the left are the excitation transmitter — a circular patch antenna — and the 5 disks on the right, are the SWG. The electric field is applied between the injection point and the ground. The disks are conveniently connected at their center by a threaded rod and nuts.

The radiation of the antenna is due partly to the direct radiation of the patch, and partly to the radiation shaped by the SWG. The superposition of the two for well-chosen dimensions of the SWG results in far field radiation pattern narrower than that of the patch alone. The patch and the SWG can be modeled independently. However, the coupling between the two elements (the small coupling zone between the second and third disc) does not lend itself to analytical study, and it is necessary to use numerical

modeling to study the influence of the interval in which the radiation from the patch is partially transferred to the surface waveguide.

The patch considered alone

This type of antenna is well documented, **[2], [3], [4], [5], [6]**. The patch behaves like a resonator with quality factor Q_r depending mainly on the radiation losses.

The radiation represents the "losses" of this cavity. However, it is the useful result of the transfer of energy from the source to space, and must therefore be maximized. The bandwidth B for an SWR < 2 depends on Q_r **[4]**,

$$B = \frac{0.75}{Q_r}.$$

Since the SWG has a wide bandwidth, it is the bandwidth of the patch that limits the bandwidth of the whole antenna. It is necessary to have a significant value of h, the dielectric patch height between the first and second disk in Figure 1, and therefore a low value of Q_r — for the antenna to have a suitable bandwidth **[7]**.

The resonant frequency of the patch alone

The circular patch may be studied alone to define the convenient diameter for a working frequency **[7]**. In addition to the diameter $2r$ (second disk), its resonant frequency also depends on h. Unfortunately, the theoretical formulas are not suitable for Gun antennas. The analytical calculation of the resonant frequency assumes an infinite reflector plane. If the reflector plane is small, it is not possible to use these relations directly. We note that these formulas deviate from the experimental results for large h.

The 'a priori' choices

The adopted value of $h/r = 0.21$ results from a compromise between the bandwidth (large h) and the value of the parasitic inductance of the supply probe, which must be as low as possible.

Furthermore, we have observed through simulation that the use of a reflector with a larger diameter than the one chosen in **Figure 1**, (about one wavelength in air), increases the directivity without increasing the size too much. Thus, we will use the following two assumptions: $h/r = 0.21$, and the reflector $2r$ diameter (ground plane) is a wavelength.

Position of the signal injection point from the axis for the patch antenna alone

The distance between the axis and the insertion point is d. Three *HFSS* simulations were performed for $h/r = 0.21$ at three frequencies 0.8, 2.45, and 4.1 GHz. After optimizing the injection point to obtain a 50 Ω match, we obtain the curve in **Figure 2**.

The position of the injection point (normalized to r) depends strongly on h/r. The radiation resistance at the edge of the disk increases with frequency **[8]**. To maintain a match to the 50 Ω source as the frequency increases, the signal injection point must move closer to the axis. When considering the complete antenna, the load of the SWG decreases the radiation impedance and forces a change in the position of the injection point.

The surface waveguide – three steps

Our goal is to build an antenna with a desired directivity D or beamwidth BW. The dimensions of the SWG of a Gun antenna are determined in three successive steps.

Step 1: Select the length of the antenna needed to obtain the directivity D or beamwidth BW at the −3 dB points, assuming in this step that the SWG is very close to that of the antenna, so it will be denoted by L (or L_n) when normalized.

Step 2: determine L_n, the SWG will interact with the radiation of the patch. This interaction is optimal for one value of the index n of the virtual material.

Step 3: Physically realize the SWG so that the virtual material has the index n. For that, it is necessary to choose correctly the diameter $2a$ of the SWG disks and their spacing.

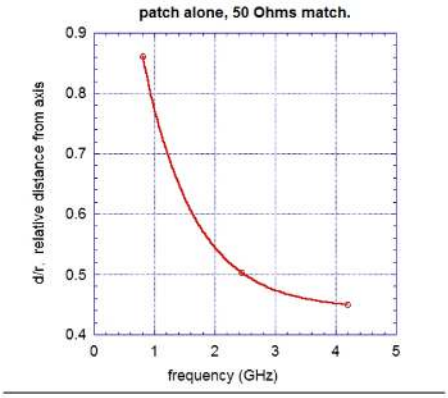

Figure 2 — The optimal position of the signal injection point for the patch antenna alone to be matched to 50 Ω. The height h of the patch normalized to the radius is h/r=0.21.

Step 1: Directivity D determines the antenna length L.

D and BW are linked **[9]**. For a half power beamwidth we have the simplified relation,

$$D = \frac{16}{BW^2}$$

where D is a linear value, and BW is in radians. The directivity and thus the beamwidth will determine the length of the SWG. This length L is normalized to λ_0 by

$$L_n = \frac{L}{\lambda_0}$$

For this, graphical aids exist **[10], [11]** (**Figure 3**); the relation between L_n and BW in radians,

$$BW = \frac{0.96}{\sqrt{L_n}}.$$

Step 2: The length of the SWG defines the propagation index

Provided that the spacing between the disks is not too large (< 0.3 λ_0), the SWG can be considered as a continuous dielectric cylinder of index n, capable of supporting a wave and radiating only at the discontinuities — excitation and end face — as would a cylindrical waveguide, and thus it preserves the polarization of the wave present at the excitation **[12]**. In the dielectric guide, the propagation index is defined as in optics,

$$n = \frac{c}{v_m} = \frac{\lambda_0}{\lambda_m}$$

where $n > 1$ and v_m is the velocity of the slowed wave, and λ_m is the wavelength in

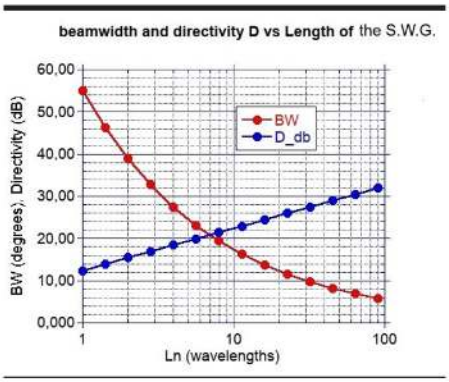

Figure 3 — The descending trace shows the beamwidth, while the ascending trace shows the directivity, as a function of the normalized length of the SWG, nearly the length of the antenna.

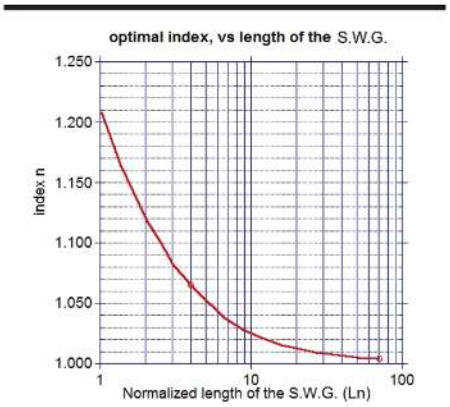

Figure 4 — The index n vs. the normalized length L_n of the SWG.

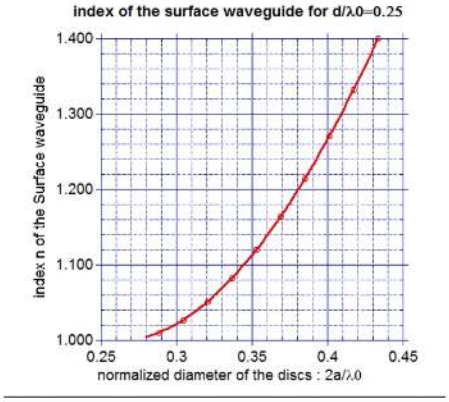

Figure 5 — Index n vs. normalized disc diameter based on Schefer reference data.

the "virtual dielectric cylinder." The optimal directivity couples the length L_n and the index n of the SWG.

We are usually interested in directivity, which we try to maximize. The superposition of the two waves — one emitted by the patch at speed c, and the one guided by the SWG at propagation speed v_m — will produce in the far field a more directive radiation than the one from the patch alone. For this to happen, a phase relation must exist at the end of the SWG between these two waves, thus between v_m and c, and an optimal value of n. Hansen and Woodyard **[13]**, have shown that for an SWG of length large in terms of λ_0, the directivity is maximum when the index value is,

$$n = 1 + \frac{0.465}{L_n} .$$

This theoretical value of the index remains the basis of calculations for this type of antenna, but small corrections have been made **[14]**, **[15]**.

The results of later work on these antennas were obtained under quite different calculation and measurement conditions. In **Figure 4**, we plotted the value of the index n versus the normalized length of the SWG from **[10]**. We have used this rule in the following, to get the best directivity for the Gun antennas.

Step 3: Choosing the SWG disk size

The director elements are not considered individually in the SWG, which is globally characterized by its index n. However, as expected, the value of the index n of the dummy material depends on its geometry **[15], [16], [17]**. A theoretical and experimental study was carried out by Schefer **[18]**. To obtain the same index n of the artificial dielectric, it is possible to play on two parameters: the diameter of the disks $2a$, and their spacing d, which define the propagation speed v_m. For convenience, we chose a 0.25 λ_0 spacing and interpolated the plots of Schefer to get the diameter $2a$ of the SWG disks. The result is plotted in **Figure 5**.

Study of a Gun antenna by simulation

In order to communicate in the 2.45 GHz band (λ_0 =122.45 mm), an antenna of this type was previously simulated by the finite element method using *HFSS* software. The starting point for the calculation of the dimensions of the elements is homothetic from **Figure 1**, see **[1]**, for the frequency 2.45 GHz. However, the relative patch height h/r = 0.21, and the first SWG disk has the same diameter as the others. **Figure 6** shows all the results obtained. The adopted dimensions are as follows for a short SWG:

• diameter $2r$ of the patch is 66.05 mm,

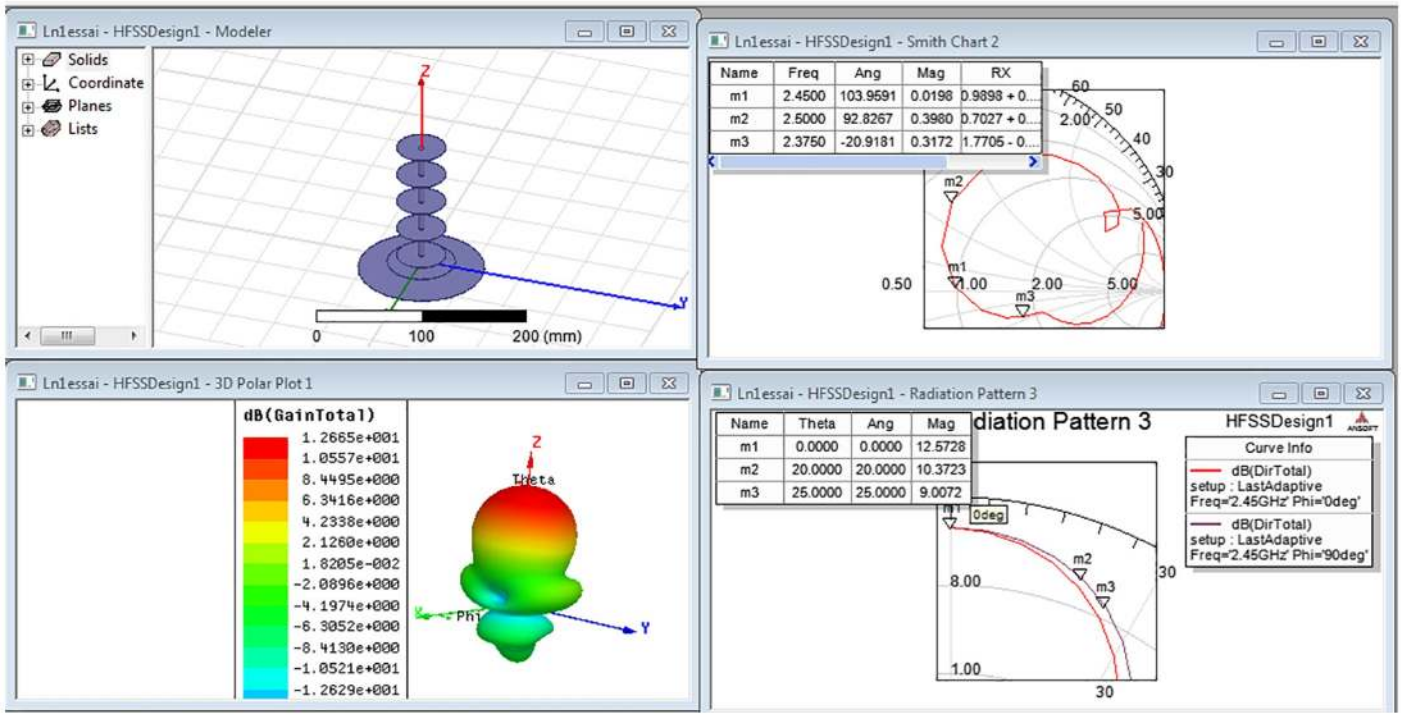

Figure 6 — Results of the simulation for the chosen dimensions. The left-top window shows the antenna with SWG of a wavelength. The right-top window shows the reflection coefficient variation with frequency. The left-bottom shows the radiation pattern in 3D. The window on the right-bottom presents the radiation pattern showing the beamwidth angle in the two planes parallel to the axis.

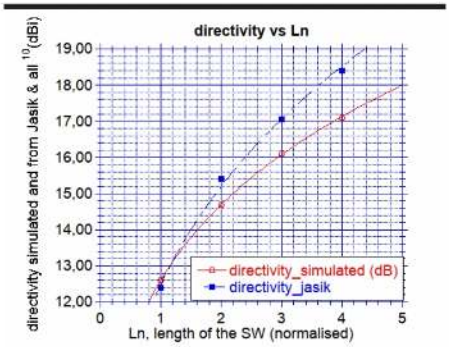

Figure 7 — The directivity (dBi) as a function of antenna length provided by the simulation is not linear. Lengthening the antenna results in more side lobes.

```
Dimensions of a Gun Antenna

Working Frequency: 2.45 GHz
Wavelength: 122.45 mm
length of the SWG: 1*Wavelength
index of the SWG:1.231
Full length of the antenna: 137.0 mm
*****************************************
thickness of the discs: 0.5 mm, non critical
axis diameter: 5.9 mm or the closest available
patch diameter : 66.05 mm ($)
distance from the center of the SMA connector to the axis :14.97 mm ($)
reflector diameter : 122.4 mm
distance between patch and reflector: 6.93 mm ($)
space between the patch and the first disc of the SWG : 7.65 mm
diameter of the SWG discs: 47.7 mm
distance between the SWG discs: 30.6 mm
*****************************************

expected directivity :12.6dB

($) précision : +-0.5% of the Wavelength
```

Figure 8 — An example of using the calculation software for the case considered above: an antenna for the 2.45 GHz band.

- distance d from the injection point (center of the connector) to the antenna axis is 14.97 mm,
- index of the virtual dielectric is $n = 1.231$,
- SWG disc diameter is $0.385\lambda_0$ (47.7 mm).

We see that the directivity reaches 12.6 dB, for an aperture at −3 dB BW close to 44°. The approximate formula $D = 16/BW^2$ gives 12 dB. The SWR<2 bandwidth is 5%.

Simulation

Thanks to the simulation, the dimensioning of a Gun antenna can be made over a wide frequency band. Subsequently, for different frequencies between 0.8 and 4.2 GHz, and lengths L_n of the SWG ranges from 1 to 4 times the free space wavelength. Analogous simulations using *HFSS* have been performed, to obtain a kind of database. With the objective to match the 50 Ω antenna to the computational frequency, the patch diameter, and the position of the injection point needed in these different cases could be determined. The optimal patch size is not affected by the length of the SWG, which was expected, while the position of the injection point

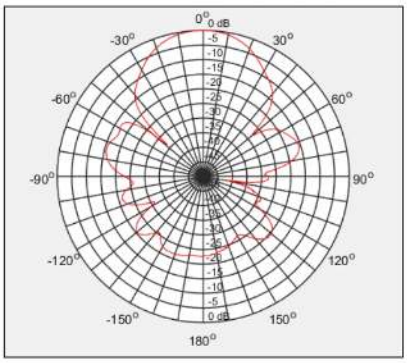

Figure 9 — Measured radiation pattern of the Gun antenna. The maximum gain is 12 dB ±0.5 dB.

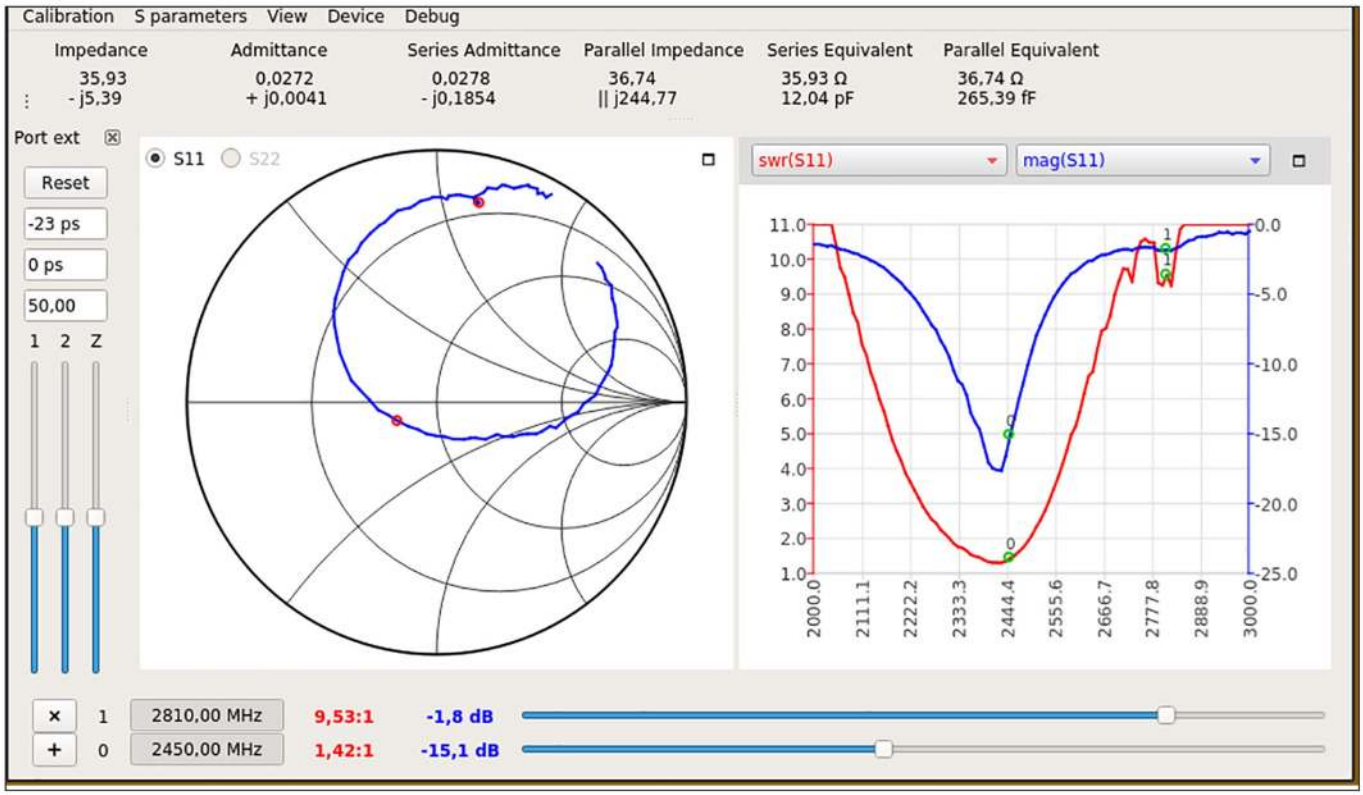

Figure 10 — Measured reflection coefficient vs. frequency at the input of the antenna. In the right panel the inner narrower curve is |S11| in dB (right scale), the outer curve is SWR (left scale).

depends on it, because of the dissipative load that constitutes the SWG.

We were able to obtain by 3D simulation, a mathematical model of these parameters of the patch diameter and position of the injection point, depending on the frequency and the length chosen for the SWG. By also modeling the obtained curves for the SWG index and diameter of the disks (**Figures 4 and 5**), we have what is necessary to establish a software program to calculate all the dimensions of a Gun antenna.

The directivity increases with the length of the antenna. For a length of $4\lambda_0$, a directivity of the order of 17 dB — close to that provided by a pyramidal or conical antenna — can be achieved (**Figure 7**) for a smaller footprint, but with a smaller bandwidth. The growth with length was expected, but it is somewhat lower than predicted by Jasik **[10]**. It does not appear that lengthening beyond $4\lambda_0$ is very beneficial.

A first version of software to calculate all dimensions of a Gun antenna (**Figure 8**) has been written in Python3 language. It is freely available at **arrl.org/QEXfiles** as a complement to this article.

Construction

The construction does not present any particular mechanical difficulty but requires some care, particularly near 4 GHz. For example, at this frequency, an error of 0.5% on the diameter of 40.6 mm (+0.2 mm) increases the modulus of the reflection coefficient from 0.02 to 0.085 (SWR from 1.04 to 1.186).

The losses in the metal remain low and steel can be used. Aluminum is easy to machine but should be avoided for the patch, which requires a soldered connection. Copper is the best electrically but easily deformed for small thicknesses. Brass could be preferred.

To position the input SMA connector, it is convenient to screw the patch disk and its reflector together, then drill a small diameter hole (about 1 mm) in this assembly at the correct distance from the axis, that will be used for the wire connecting to the patch disk. It is best to avoid nuts and washers inside the patch because they degrade the antenna match to the source.

There are videos on the internet that can help **[19]**.

Measurements

Measurement of the radiation pattern: An antenna was built to the exact dimensions of the simulation model. The radiation pattern was measured in an anechoic chamber, see **Figure 9**. The gain (directivity + losses) of 12 dBi was measured in comparison to that of a reference pyramidal horn antenna.

Measurement of the reflection coefficient at the input of the antenna: The measurements show that the antenna is tuned to 2,432 MHz compared to an expected 2,450 MHz. This deviation is currently being analyzed. The SWR is less than 2:1 in a7.7% band, see **Figure 10**.

Conclusions

The Gun or disk Yagi antenna is well suited for applications between 1 and 4 GHz. The lower frequencies are penalized by an excessive size of the reflector, and possibly wind loading. Higher frequencies require high mechanical precision.

Advantages: Antennas are easy and fast to build, no balun is necessary. The construction tolerates small dimensional deviations of the SWG. The gain/dimensions ratio is favorable compared to horns.

Disadvantages: The bandwidth is relatively narrow band because of the excitation by a patch, so the dimensions of the patch must be precise. The diameter of the disk, the position of the injection point, the height h of the patch above the reflector disk must be well controlled.

Acknowledgments

This work was carried out thanks to the availability of measurement facilities (anechoic chamber, vector network analyzers) and calculation facilities (3D HFSS simulation) at the Institut Universitaire de Technologie of Ville d'Avray (University of Paris Nanterre).

Jean-Claude Hénaux worked on Josephson effects in superconductive junctions and received his PhD in 1983 from the Paris Sud-Orsay University. As a professor at Paris Sud-Orsay University and Paris Ouest Nanterre, he was involved in the design and measurements on microwave GaAs ICs and taught electronics, and particularly microwave electronics. He is now retired and helps (for pleasure) with student microwave projects at the Ville d'Avray Institute of Technology.

Franck Daout received his MS and PhD degrees in electronics from the University of Nantes (France) in 1996. From 1997 to 1999 he was a Research Engineer at the French Naval Academy, at Brest, France, Groupe de Traitement du Signal in the sonar team. In 1999, he became an assistant professor at the University of Paris-Ouest Nanterre la Defense. His research and teaching courses are in the fields of electromagnetic wave propagation, microwave and signal processing. Currently, he works on radar systems at the Systemes et Applications des Technologies de l'Information et de l'Energie (SATIE) Laboratory, ENS Cachan France.

Notes

[1] **https://www.youtube.com/watch?v=zKcz6rEXamc**.
[2] R. A. Saïnati, *C.A.D. of Microstrip Antennas for Wireless Applications*, Artech House, Chap. 3-10.
[3] J. R. James, P.S. Hall, C. Wood, "Microstrip Antennas, Theory and Design," *IEE Electromagnetic Wave Series 12.*
[4] P. F. Combes, *Micro-Ondes -2*, Dunod. Chap. 15.
[5] R. Garg, P. Barthia, I. Bahl, A. Ittipiboon, *Microstrip Antenna Design Handbook*, Artech House.
[6] J. L. Volakis, T. F. Eibert, *Antenna Engineering Handbook*, McGraw Hill, 2007, Chap. 7.7.
[7] L. C. Shen, S. A. Long, M. Allerding, and M. Walton, "Resonant Frequency of a Circular Disk Printed-Circuit Antenna," *IEEE Trans. Antennas and Propagation*, Vol. 25.
[8] C. A. Balanis, *Antenna Theory, Analysis, and Design*, (4th. Ed) J. Wiley 2016.
[9] S. J. Orfanidis, *Electromagnetic Waves and Antennas*, Rutgers University, Chap. 16-2.
[10] R. C. Johnson, H. Jasik, *Antenna Engineering Handbook*, McGraw.Hill,1993. Chap.12.
[11] T. A. Milligan, *Modern Antenna Design*, J. Wiley & Sons 2005. Chap. 10.
[12] C. H. Chandler, "An Investigation of Dielectric Rod as Waveguide," *J. Appl. Phys.* Vol. 20, Dec. 1949 pp: 118-192.
[13] W. W. Hansen, J. R. Woodyard, "A New Principle in Directional Antenna Design," *Proceedings of the Institute of Radio Engineers*, Vol. 26, No.3, 1938, pp: 333-336.
[14] H. Bach, "Applicability of Hansen-Woodyard Condition," *Proceedings of the IEEE*, Vol. 119, No. 1, Jan. 1972, pp. 38-40.
[15] H. W. Ehrenspeck, H. Poehler, "A New Method for Obtaining Maximum gain from Yagi Antennas," *IRE Transactions on Antennas and Propagation*, (11/1959), pp.379-386.
[16] G. Piefke, "The Transmission Characteristics of a Corrugated Guide," *IRE Transactions on Antennas and Propagation*, Dec. 1959, pp: S183-S190.
[17] A. D. Olver, F. F. Dubrovka, C. G. Parini, "Propagation and Radiation Characteristics of the Disc-on Rod Antenna," *Radio Science*, Vol. 19, No 6, Nov.-Dec. 1984, pp: 1439-1444.
[18] J. Schefer, "Plane Waves on a Periodic Structure of Circular Disks and Their Application to Surface Wave Antennas," *IRE Transactions on Microwave Theory and Techniques*, Nov. 1962, pp: 595-592.
[19] **https://www.youtube.com/watch?v=W5DskYocQRk**.

Dr. Sam Green, WØPCE

11439 Daykin Dr., Saint Louis, MO 63146; **w0pce@arrl.net**

Sweep Generator Measurement System – Take 5

This versatile piece of test equipment performs many useful functions.

Let's look at what you can do with this combination of elements when you program a computer to control them to operate together. The elements are:

- Programmable oscillator
- Logarithmic RF Detector (Log Detector)
- Digital to Analog Converter (DAC)
- Analog to Digital Converter (ADC).

In previous implementations, the computer was a PC and parallel port pins connected to these **[1]**, **[2]**, **[3]** elements. In a 4th paper, "Fully Automated Sweep Generator Measurement System - Take 4," Jan., 2022 *CQ* Magazine, an Arduino Uno, an LCD display, and a PS2 keyboard replace the PC. Here, all circuitry moves to an Arduino shield.

The programmable oscillator is either an Analog Devices AD9851 that generates a near sine wave over a frequency range of 0 to 60 MHz by Direct Digital Synthesis (DDS) or one of the many types of Silicon Devices Si570 Programmable Crystal Oscillators (PXO) that generate a logic level (square wave) waveform over a frequency range beginning at 10 MHz up to various frequencies in the VHF and UHF range, depending on the particular version of Si570. The least expensive CMOS version is the Si570CAC that sweeps up to 157 MHz. The Si570BAB sweeps continuously up to 810 MHz.

The Arduino sketches (software programs) control the AD9851 DDS or the Si570 to step through successive frequencies to "sweep" from a lower frequency to a higher frequency in controllable frequency steps.

A Log Detector provides a very large dynamic range measurement of the swept RF that passes through a unit undergoing testing. Analog Devices specifies the AD8307 to 500 MHz. With extra-large input capacitors in the circuit, frequency response extends down into the audio range.

As the frequency sweep progresses from minimum to maximum, the sketch also programs the DAC to output a corresponding voltage ramp that starts from a minimum negative voltage and increases in controllable steps to a maximum positive voltage. The voltage ramp serves to control horizontal deflection on an oscilloscope while it displays the amplitude response to the swept RF signal on the vertical axis. This is useful for the real time display of repetitive swept response. The voltage ramp also serves as a swept voltage source for evaluating the transfer function response (divide voltage output by voltage input) of a circuit or circuit element.

The ADC measures the voltage from the Log Detector on one input and software converts the result to power level in dBm (decibels with a 1 mW reference). The ADC also measures the voltage in response to the output from the DAC in transfer function mode on the other input.

Operating Modes

1 – *Repeat RF Sweep:* The RF source repeatedly sweeps across a settable frequency range as a voltage output ramps between negative and positive limits to provide horizontal sweep for an oscilloscope that displays the response of a high frequency logarithmic detector to the RF input through a circuit under test.

2 – *Single RF Sweep & Measure:* The RF source sweeps one time across a settable frequency range as the ADC measures the voltage from the Log Detector and provides data for plotting.

3 – *Transfer Function:* The voltage source sweeps one time across a settable

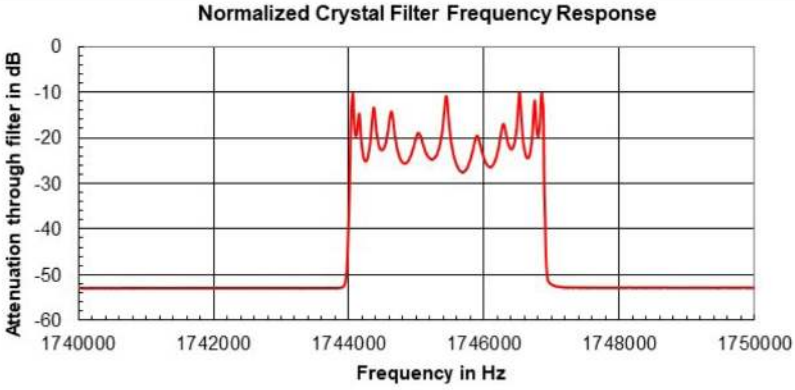

Figure 1 — An example of RF sweep generator use.

voltage range as the ADC measures the responding voltage from a circuit under test and provides the data for plotting.

An example of RF sweep generator use appears in **Figure 1** where the frequency is swept over a narrow range a single time to get the response of a crystal filter while the ADC measures the voltage from the Log Detector. The program outputs text of frequency and voltage measurements ready to plot in a spreadsheet.

Examples of using the transfer function to generate a swept voltage response appear in **Figure 2**. Connect the DAC output to the ADC input to generate the calibration

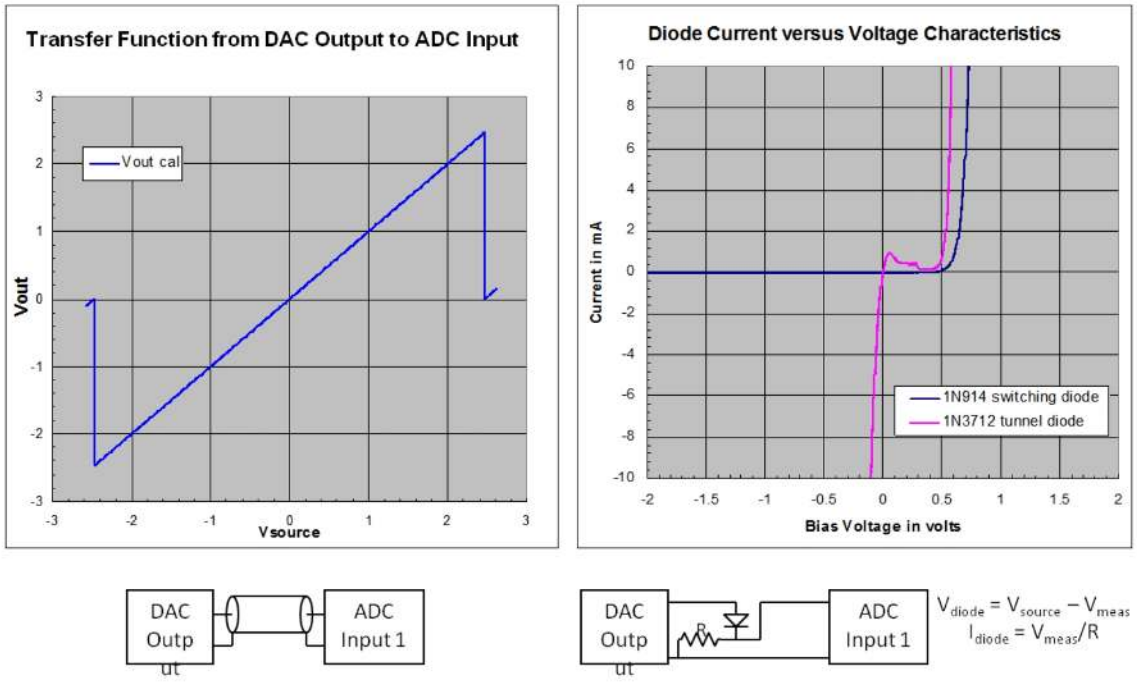

Figure 2 — Examples of using the transfer function to generate a swept voltage response.

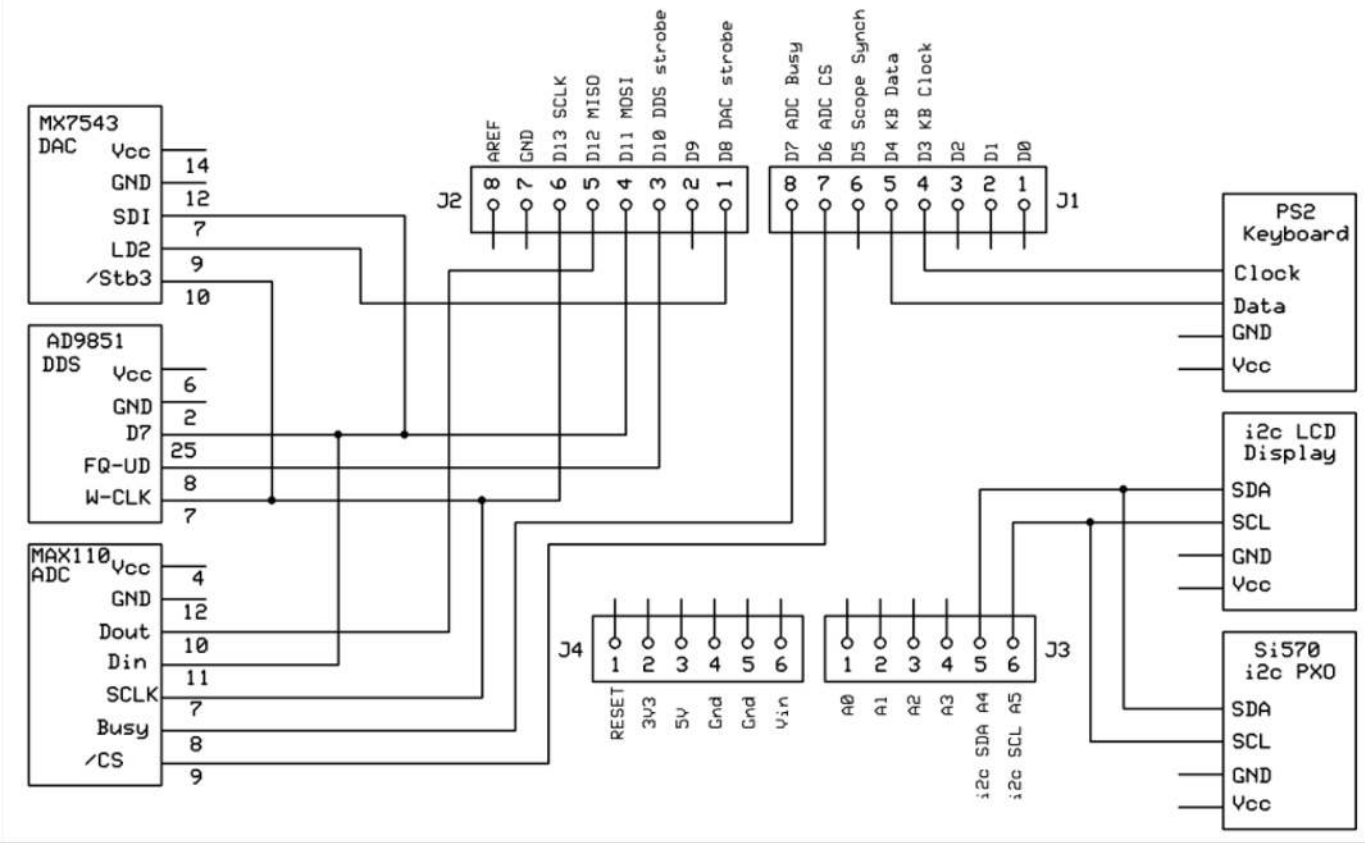

Figure 3 — Interconnections between the Arduino Uno and the functions it controls.

on the left. Connect the ADC and DAC to a diode and current sensing resistor as shown to generate the current versus voltage characteristic curves on the right.

Architecture

Figure 3 shows the interconnections between the Arduino Uno and the functions it controls. A "shield" plugs into the main Arduino connectors J1 – J4. The Arduino community calls a plug-in daughter card a shield. All circuitry is on or connects to the shield.

A PS2 keyboard connects to J9 on the shield for simple numeric data entry. A useful little adapter board from AliExpress greatly simplifies this connection **[4]**. Thanks to PJRC for the PS2Keyboard Library **[5]**. This should also work with a USB keyboard in PS2 compatibility mode, but that doesn't work for me.

The LCD display **[6]** connects to J8 on the shield and communicates via the Inter-Integrated Circuit (I2C) protocol over 2 digital pins by means of an adapter board that attaches to the original standard LCD display that requires 6 digital pins.

The Arduino Uno has 13 digital I/O pins, 2 of which I reserve for serial communications, plus 6 more analog pins that work fine as digital I/O pins. I used 2 pins for the PS2 keyboard and 2 for the I2C LCD display. The 2 I2C pins are SDA and SCK and control any other I2C accessory if it operates at a different address. These same 2 pins control the Si570 as well. The Arduino environment includes a library of functions to control I2C devices.

The DDS, DAC, and ADC communicate via the Serial Peripheral Interface (SPI) protocol. The Arduino environment also includes a library of functions to control SPI devices through dedicated pins for MISO, MOSI, and SCLK. This allows use of these pins in common. Only the ADC uses MISO as well as a busy signal. Then each SPI device needs a separate enable line to select the particular device. With everything hooked up and running, including a dedicated discrete oscilloscope trigger for diagnostics or control, there are still 5 unused pins, A0 – A3 and D9, available for future expansion. Some Arduino boards, including a discontinued version **[7]** of the Uno, also allow access to additional pins A6 and A7.

RF Sources

The Analog Devices AD9851 DDS sweeps from 0 – 60 MHz. The NJQRP DDS-60 daughter card with an AD9851 DDS is still available **[8]** and plugs into J11 of the shield. It operates by synthesizing 10 bit approximations of a sine wave to provide readily filtered sinusoidal waveforms. Other inexpensive boards with AD9851 or AD9850 (0 – 30 MHz) DDS chips are available on **AliExpress.com**, but these do not include an amplifier to raise the output

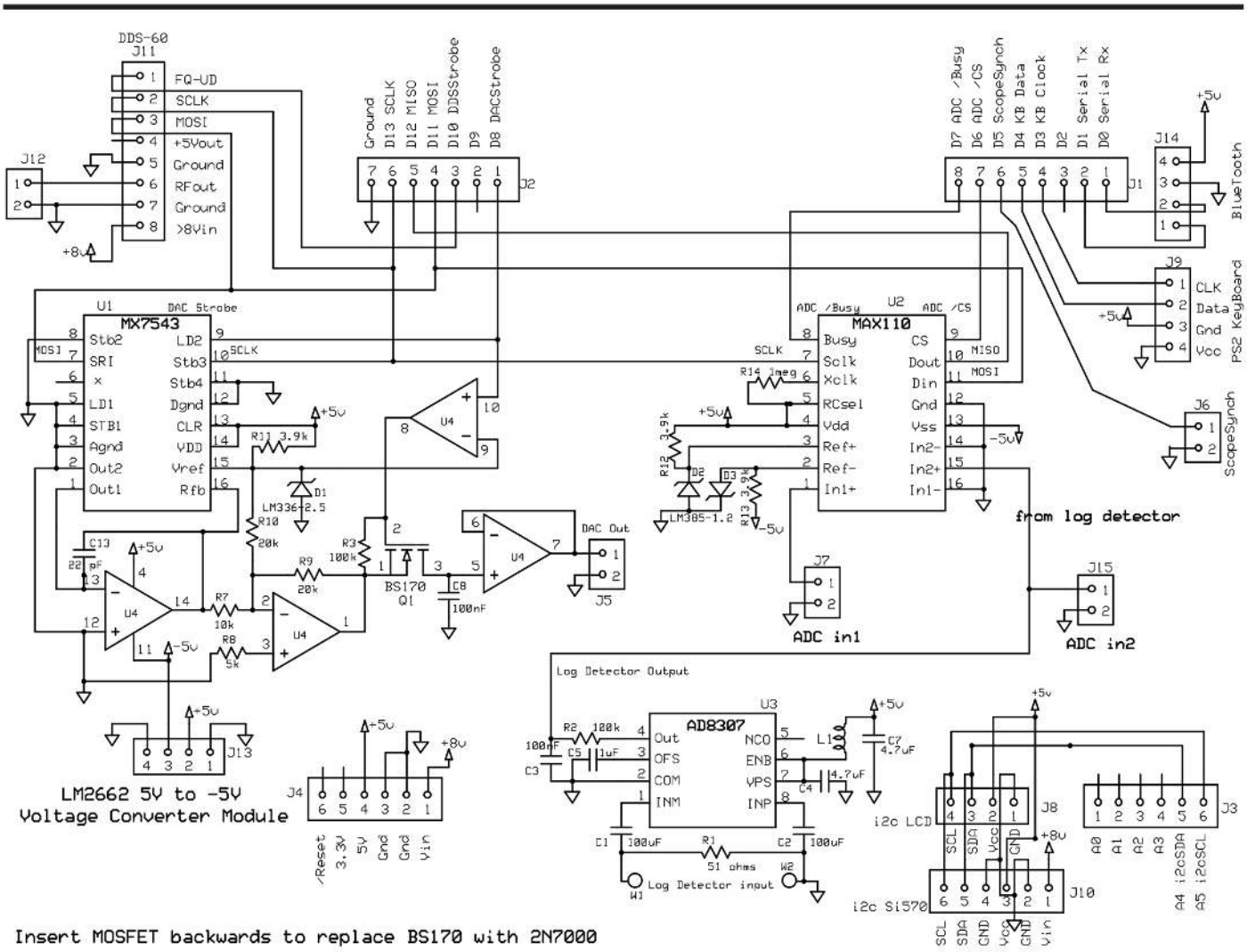

Figure 4 — Schematic diagram of the sweep generator shield.

level. Connections can be brought to these other DDS boards from J11. The AD9850 requires a single bit change and a different upper frequency limit in the sketch.

Dave Brainerd, WB6DHW, offers an inexpensive little daughter card **[9]** at **wb6dh.com** that mounts the Si570. The Si570 PXO sweeps from 10.0 MHz up to various VHF/UHF limits depending on the particular version. Mine is an Si570BAA and sweeps continuously up to 935 MHz and higher, but with gaps in the range. The Si570BAB sweeps continuously up to 810 MHz. The least expensive CMOS version of the Si570 sweeps up to 157 MHz.

Note that the Si570 module must have an onboard 3.3 V voltage regulator and logic level translators for the clock and data lines, as the Si570 cannot handle a Vcc of +5 V.

Differences between the Analog Devices DDS and the Silicon Labs Si570 are many. One major difference is that the Si570 provides logic level outputs rather than synthesized sinusoidal waves. However, I have never observed a harmonic problem when sweeping with a non-sinusoidal waveform.

Another major difference is that control of the Si570 is through an I2C interface rather than the serial SPI (or parallel) interfaces of the AD9850 and AD9851.

Thanks to Peter B. Marks for the DDS SPI control routine **[10]**. Thanks to Nick Kennedy, WA5BDU, for the Si570 I2C control routine **[11]**.

The functions that communicate via SPI have common clock and data lines, and the functions that communicate via I2C have common clock and data lines.

ADC and DAC

The best reference I found for controlling the ADC and DAC with SPI **[12]** wasn't very helpful, because the MAX110 and MX7543 are not at all similar to the ADC and DAC in that article, but it was a starting point.

I program the DAC to generate a ramp analog voltage to provide a driving signal for the transfer function measurement (output voltage versus input voltage) and to use as a horizontal oscilloscope sweep for displaying response to repetitive voltage and RF frequency sweeps.

The ADC measures voltage at either of two inputs with 12 – 14 bit resolution. I select 13 bit operation. One input is for transfer function measurements. A logarithmic detector to measure RF signal level from a unit under test feeds the second ADC input.

Logarithmic RF Detector

The AD8307 logarithmic RF detector is suitable for the AD9851 DDS and the lower frequency Si570 variants. Frequency response is up to 500 MHz and the dynamic range is from –78 to +10 dBm within 1 dB.

An ADL5513 logarithmic RF detector with frequency response up to 4 GHz and a dynamic range from –58 to +6 dBm within 1 dB would much better suit the higher frequency Si570 variants, but it should be external in a shielded case. I made no provision on the Arduino shield except for a 2nd input connector to the ADC.

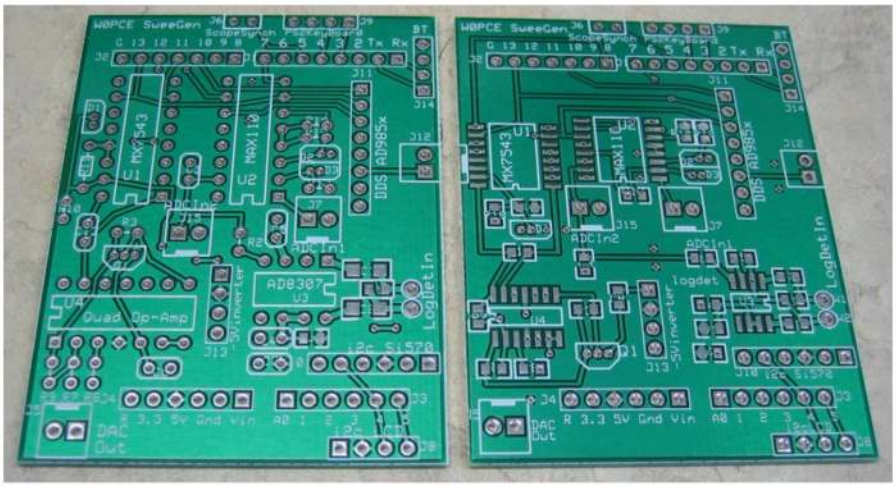

Surface Mount Component Version Surface Mount Component Version

Figure 5 — Two versions of the Arduino shield PC board.

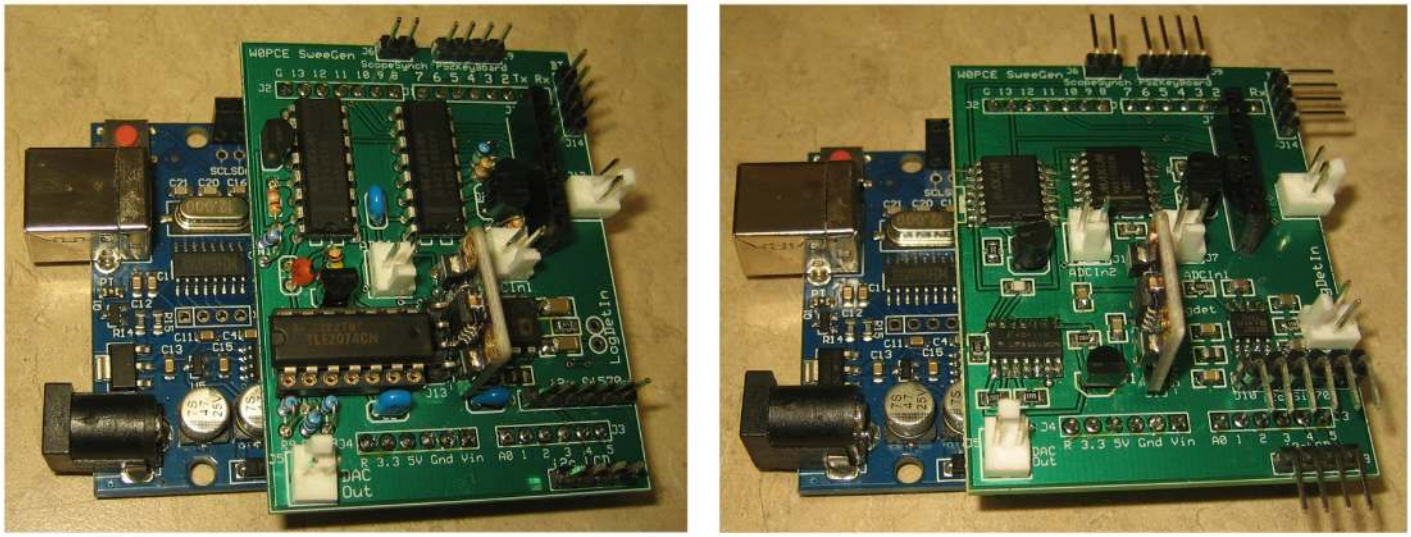

Figure 6 — Through-hole (A) and surface mount (B) shield versions on an Arduino Uno without attached accessories.

Hardware

Figure 4 shows the complete schematic diagram of the sweep generator shield. The operational amplifiers and the ADC require a negative supply voltage. Rather than put LM2662 voltage converter circuitry on the shield, I bought a preassembled LM2662 module **[13]** and mounted it vertically.

The DDS can be either on the NJQRP daughter card that plugs into the shield or on one of the several AD9851 modules available from AliExpress and others **[14]** and connect by M–F cables to the same connector for power and SPI data.

The Si570 module from WB6DHW connects to connector J10 with a 2 pin F–F cable for power and a 4 pin F–F cable for I2C data.

The PS2 keyboard adapter connects to connector J9 with a 4 pin F–F cable. The LCD display connects to connector J8 with a 4 pin F–F cable for I2C data. The Bluetooth module connects to connector J14 with a 4 pin F–F cable.

Figure 5 shows the two versions of the Arduino shield PC board. One primarily uses through-hole components, with the exception of the high frequency Log Detector. The second primarily uses surface mount components, with the exception of the reference diodes and the sample-and-hold MOSFET.

Figure 6A shows a photo of the through-hole version and **Figure 6B** shows the surface mount version of shields on an Arduino Uno without attached accessories. Either accepts an AD9851 (or AD9850) direct digital synthesis RF source or an Si570 programmable oscillator source with a corresponding sketch (software load).

Figure 7 shows a photo of the surface mount shield with accessories attached and operating. These include the I2C WB6DHW Si570 board, a 4 line by 20 character I2C LCD display, an HC-05 Bluetooth module, and a PS2 keyboard connection. Note the cute little adapter board from AliExpress **[15]** for the PS2 connector.

DAC Software Driver

The short subroutine of **Table A** tells the Arduino to send a command to the DAC via SPI. This subroutine receives an integer value from 0 – 4095 to write to the DAC. Note the built-in SPI functions.

ADC Software Driver

This corresponding subroutine (**Table B**) tells the Arduino to send a command to the

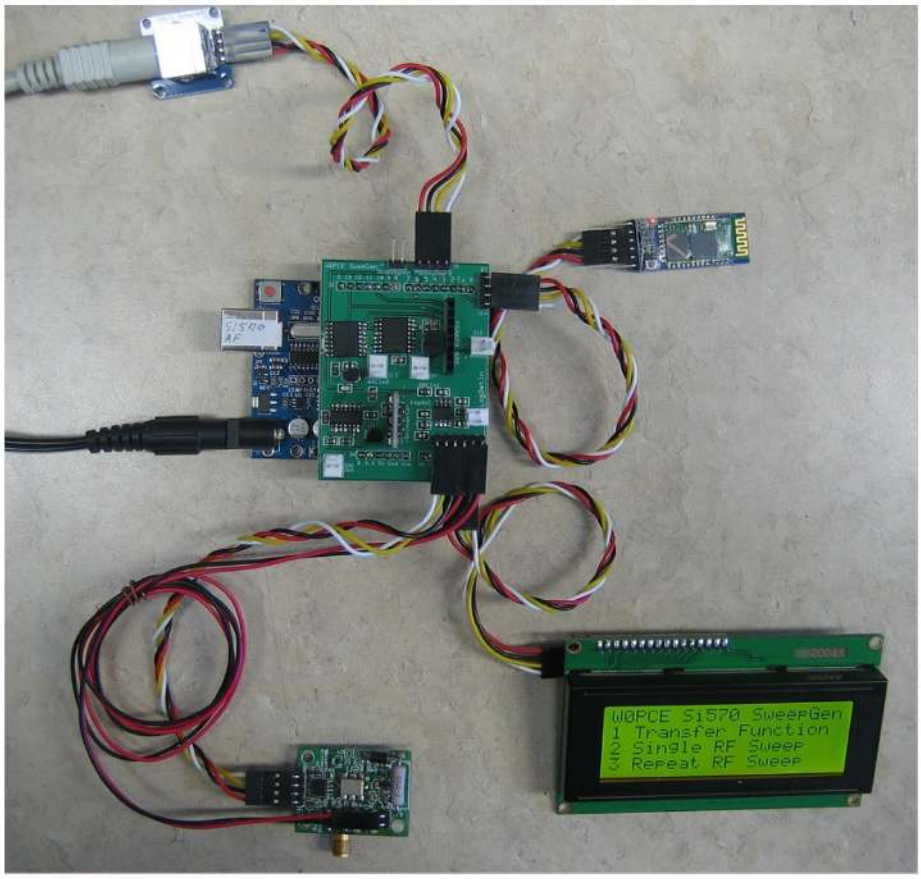

Figure 7 — Surface mount shield with accessories attached and operating.

Table A – Subroutine.

```
void DACwrite(int value) {
 int byte_0, byte_1;
 SPI.beginTransaction(SPISettings(10000000, MSBFIRST,S PI_MODE3));
 SPI.begin();
 digitalWrite(DACselect, LOW);
 byte_0 = (value >> 8);
 byte_1 = (value & 0xFF);
 SPI.transfer(byte_0);
 SPI.transfer(byte_1);
 digitalWrite(DACselect, HIGH);

}
```

Table B – Subroutine.

```
uint16_t readADC(uint16_t commandword) {
 byte commandMSB = (commandword & 0xff00)>>8 ;
 byte commandLSB = (commandword & 0x00ff) ;

 SPI.beginTransaction(SPISettings(10000, MSBFIRST, SPI_MODE3));
 SPI.begin();
 digitalWrite(ADCCS, LOW);
 byte msb = SPI.transfer(commandMSB);
 byte lsb = SPI.transfer(commandLSB);
 digitalWrite(ADCCS,HIGH);
 while (digitalRead(ADCbusy)== LOW);
 return ((uint16_t) msb) <<8 | lsb;                    // cast before shifting byte

}
```

Table C – Subroutine C.

```
void sendFrequency(unsigned long frequency) {                    // for AD9851 DDS
 unsigned long tuning_word = (frequency*pow(2,32))/DDS_CLOCK;
 SPI.beginTransaction(SPISettings(8000000, LSBFIRST, SPI_MODE0));
 SPI.begin();
 digitalWrite(DDSstrobe, LOW);
 SPI.transfer(tuning_word);
 SPI.transfer(tuning_word >> 8);
 SPI.transfer(tuning_word >> 16);
 SPI.transfer(tuning_word >> 24);
 SPI.transfer(0x01);                                             // 0x00 for AD9850
 digitalWrite(DDSstrobe, HIGH);
}
```

Table D – Subroutine D.

```
byte send_new_freq() {
 Wire.begin();                          // Initialize I2C for Si570 means as master
 freeze_dco();
 byte errorbyte = 1;
 int count = 0;
 char x;
 while(errorbyte != 0) {
 Wire.beginTransmission(SI570_ADDRESS);
 Wire.write(7);                         // send lowest register address to slave
 for (x=0; x < 6; x++) Wire.write(SiRegs[x]);
 errorbyte = Wire.endTransmission();
 count++ ;
 }
 unfreeze();
 centerRFREQ = RFREQ;                   // re-centered by freezing
 return count;
}
```

ADC via SPI to read a voltage input. Note that the *commandword* specifies the number of bits of resolution, which input to read, and other parameters. This looks simple, so I'm embarrassed to admit it took 2 full weeks to make this work.

AD9851 DDS Software Driver

The software that tells the Arduino to send a frequency command to the DDS via SPI looks like this (**Table C**). The 4th byte changes from 1 to 0 to use an AD9850 in place of the AD9851.

Note that each of the SPI devices requires different SPI parameters, so these are specified at the entry to each of the subroutines rather than in *setup()*.

Si570 Software Driver

The software (**Table D**) that tells the Arduino to control the Si570 PXO is neither simple nor compact. This main subroutine calls many others.

Arduino Program

The complete commented sketch for this project along with ExpressPCB layout files for the shields is available on request from the author. The sketch presently uses only half of the available program area, so there is plenty of room for changes and improvements. For example, software for both the AD9851 DDS and the Si570 would fit, and either could be driven with expanded menus.

Data entry is currently in integer hertz for lower and upper frequency sweep points but is in floating point with decimal for lower and upper voltage sweep points. You can change this. You may not like the layout of my menus, but you can change them. Arduinos are wonderful in this way.

A quirk I should mention is that I use logarithmic sweep where frequency steps are a multiple of one plus a small number rather than an addition in fixed frequency increments. This gives more useful data on wide sweeps and doesn't matter for narrow sweeps. Also the main for-loops sweep the DAC output and compute the appropriate frequency steps, rather than sweeping frequency directly.

Menus

The main menu on starting or on reset fits a 4 line by 20 character display and looks like this. Entering 1, 2, or 3 selects the next menu.

W0PCE Si570 SweepGen
1 Transfer Function
2 Single RF Sweep
3 Repeat RF Sweep

For *Transfer Function*, the display asks the user to enter the start level in volts while showing the entry, then the stop level, then the number of steps. Suitable entries might be:

–2.41 Enter
2.41 Enter
4095 Enter

When entered, the display summarizes the entries and begins the single sweep. Frequency and measured data print in lists of numbers from the serial Tx port. On completion, a software reset returns the user to the main menu.

For *Single RF Sweep*, the display asks the user to enter the start level in hertz while showing the entry, then the stop level, then the number of steps. Suitable entries might be:

10000000 Enter
150000000 Enter
4095 Enter

When entered, the display summarizes the entries and begins the single sweep. Frequency and measured data print in lists of numbers from the serial Tx port. On completion, a software reset returns the user to the main menu.

For *Repeat RF Sweep*, the display asks the user to enter the start level in hertz while showing the entry, then the stop level, then the number of steps. Suitable entries are the same as for *Single RF Sweep*. This runs until manually stopped by pressing any keyboard key to initiate a software reset that returns the user to the main menu. *Repeat RF Sweep* mode also causes a corresponding repeat analog sweep of a voltage ramp from the DAC over the full range from negative to positive.

Data Output for Plotting

The data still must arrive as a text file at a real PC for plotting in a spreadsheet. The serial output data arrives at both the serial Tx pin and the USB of the Arduino.

If the Arduino connects to a PC via a USB cable, the PC can capture the serial data with the Serial Monitor built into the Arduino programming environment or with *PuTTY* **[16]**, a terminal program.

A nice alternative is bringing the serial Tx signal to an HC-05 Bluetooth module.

Then a laptop with Bluetooth running *PuTTY* captures the data. Increase the HC-05 baud rate to 115200 for better response, or use it unchanged at 9600 baud, but correct the baud rate in the sketch. An HC-05 Bluetooth module connects with a 4 pin F–F cable to connector J14 on the shield.

Sample and Hold

The DAC outputs a narrow glitch when it transitions between output levels. This has no effect on Transfer Function measurements that are taken after the glitch, but it blurs the deflected spot horizontally when viewing repetitive waveforms on an oscilloscope. I added the sample and hold circuit consisting of the MOSFET and a couple operational amplifiers to remove the glitch in this latest version.

Summary

This instrument and its predecessors prove useful in making precision laboratory measurements. I found a 4 × 4 keyboard with a single analog output **[17]** that may replace the PS2 Keyboard in a future version. I love this hobby!

Dr. Sam Green, WØPCE, is a retired aerospace engineer living in Saint Louis, Missouri. He holds undergraduate and graduate degrees in Electronic Engineering from Northwestern University in Evanston and the University of Illinois at Urbana respectively. Sam specialized in free-space optical and fiber optical data communications and photonics. He now designs targets for guns with laser bullets. Sam became KN9KEQ and K9KEQ in 1957, while a high school freshman in Skokie, Illinois, where he was a Skokie Six Meter Indian. Sam held a Technician class license for 36 years before upgrading to Amateur Extra class in 1993. He is a member of ARRL, a member of the Boeing Employees Amateur Radio Society (BEARS), a member of the Saint Louis QRP Society (SLQS), and a member of the Bi-State Amateur Radio Society. Sam is a Registered Professional Engineer in Missouri and a Life Senior Member of IEEE. Eighteen US patents list Sam as inventor.

References

[1] S. Green, WØPCE, "Fully Automated DDS Sweep Generator Measurement System," *QEX* Nov./Dec. 2008, pp 13-22.
[2] S. Green, WØPCE, "A Fully Automated DDS Sweep Generator Measurement System - Take 2," *QEX* Sep./Oct. 2012, pp 3-13.
[3] S. Green, WØPCE, "A Fully Automated DDS Sweep Generator Measurement System – Take 3," *QEX* July/Aug. 2014, pp 3-11.
[4] **https://www.aliexpress.com/item/1005001379873641.html**.
[5] **https://www.pjrc.com/teensy/td_libs_PS2Keyboard.html**.
[6] **https://www.aliexpress.com/item/32991449983.html**.
[7] **https://www.aliexpress.com/item/32752122519.html**.
[8] **https://midnightdesignsolutions.com/dds60/#Overview**.
[9] **wb6dhw.com/For_Sale.html#Si570**.
[10] **blog.marxy.org/2008/05/controlling-ad9851-dds-with-arduino.html**.
[11] **pages.suddenlink.net/wa5bdu/Si570_New.ino**.
[12] **https://www.allaboutcircuits.com/projects/arduino-spi-library-ltc1286-dac714/**.
[13] **https://www.aliexpress.com/item/1005001639598862.html**.
[14] **https://www.aliexpress.com/item/33044495879.html**.
[15] **https://www.aliexpress.com/item/1005001379873641.html**.
[16] **https://www.putty.org/**.
[17] **https://www.aliexpress.com/item/32635207928.html**.

Hans J. Hartfuss, DL2MDQ and **Klaus Lohmann, DK7XL**

Am Schaeperhoff 30, 17498 Weitenhagen, Germany;
h.hartfuss@t-online.de

Godeke-Michels-Weg 12, 21762 Otterndorf, Germany;
dk7xl@t-online.de

Estimation of Ionospheric Drift Velocity by Doppler Measurements

Frequency shift determined via phase change using dedicated PowerSDR software operating the transceivers is in agreement with the drift motion derived from simultaneously performed ionograms.

The drift motion of the ionosphere has been determined by measuring the Doppler shift of a signal transmitted at 3530 kHz, receiving the space wave on locations about 300 km apart. The measurements are conducted over about eight hours, beginning in the morning. Frequency stabilized SDR transceivers have been used on both ends. The frequency shift is determined via the timely phase change by means of the dedicated PowerSDR software operating the transceivers. The results are in agreement with the drift motion as derived from ionograms performed simultaneously by a nearby scientific institution.

Introduction

We are reporting on measurements that were conducted years ago, on November 29 in 2009. Our report is triggered by two articles that appeared recently: one described the activities to establish a planet-sized network for monitoring the effects of solar activity **[1]**, and the other one **[2]** summarized a community science experiment conducted in 2019. In this experiment the time station WWV is used and the Doppler shift of a 5 MHz carrier is measured by a number of stations and the results are integrated and analyzed with the aid of powerful software. This latter experiment, although conducted with a multitude of receivers, is similar to what we did years ago in a comparatively basic way using a single receiver.

The first observations were conducted on the carrier of the German AM station Deutsche Welle on 6075 kHz. Since the station's signal was strong all over Europe and its carrier frequency was held constant to a few parts in 10^9, we used this station to calibrate the frequency of the FLEX-5000A SDR transceivers **[3]** that we were operating. The oscillators of the FLEX-5000A could as well be stabilized by injecting an external 10 MHz signal from a highly stable source, a Rubidium frequency standard **[4]** for example. This enabled us now vice versa to measure the accuracy of the AM station's carrier we were receiving.

The comparison could be performed in a simple way: receiving the AM station in DSB mode of the FLEX-5000A receiver with the dedicated PowerSDR™ software **[5]** enabled a measurement of the phase of the AM carrier compared to the highly stable carrier as generated at the same frequency in the receiver for DSB demodulation. The phase difference is displayed in a polar diagram on the PowerSDR™ display by a point in a circle, where the full circle corresponds to 360°. Observing the 6075 kHz AM station during night time with stable propagation conditions, the point in the polar plot showing the momentary phase difference is somewhat jittery, but in time average almost constant over minutes. However, in the morning hours we observed that the point in the polar diagram was going round and round indicating a continuous phase change in time over minutes and hours, thus indicating a frequency difference of up to about 0.6 Hz. Since this effect became small around noon time after that increasing again, however, with opposite sign — the point in the polar plot now rotating in opposite direction — we assumed the observation was caused by Doppler shift of the carrier frequency we were observing. Since a moving target like an airplane could be excluded, the slow downward motion of the reflecting ionospheric layer in the morning hours and its upward motion in the afternoon was supposed to be the cause of the observation. The phenomenon was drawing our interest and we decided to do a dedicated experiment to explore the findings in more detail.

The Experiment

In the final arrangement two FLEX-5000A transceivers were used, both stabilized by Rubidium frequency standards LPRO-101 by DATUM/EFRATOM, which were available as surplus but still in sufficiently good condition. Both standards were adjusted to zero beat against each other as well as against a DATUM EFRATOM 2000 GPS professional 10 MHz frequency

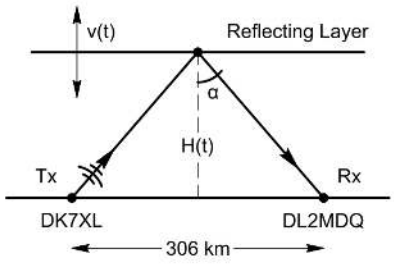

Figure 1 — Arrangement for the Doppler shift measurements. A signal is transmitted at DK7XL and received at DL2MDQ, 306 km apart. The space wave is reflected at an ionospheric layer of height H. Since this layer is moving, the signal suffers a small Doppler shift which is measured.

standard, which was available to us for test purposes. After these successful test and calibration procedures the standard sources are applied to the FLEX-5000A transceivers at the DK7XL location in grid JO43kt acting as the transmitter and at the DL2MDQ location in grid JO64qb acting as the receiver about 300 km apart (**Figure 1**). We selected a frequency in the CW part of the 80 m band at 3530 kHz since this band provides during daytime at the end of November propagation conditions such that the signal level at 100 W output power and dipole antennas on both sides clearly exceeds the S-9 level, thus enabling measurements at signal to noise ratios of typically 30 dB.

The day the experiments were conducted, on Sunday, November 29 in 2009, the radios locked to the Rubidium standards were running continuously from about 6:00 until 16:00 UTC in the afternoon. However, the transmitter at DK7XL is switched on for only about 10 minutes around full hours, the time interval we agreed on to conduct the phase and frequency measurements at DL2MDQ.

The Doppler shift as measured in the preliminary experiments at 6075 kHz amounts to 0.6 Hz in maximum. Assuming the same velocity of the moving ionospheric target, at 3530 kHz a Doppler shift not higher than about 0.3 Hz is expected. How can this small frequency offset be measured with amateur equipment just using the PowerSDR™ software in Phase Mode? It is possible by measuring the time that the point in the polar phase display completes N full circles, thus a phase change of N times 360° or N times 2π. If the time for N = 10 revolutions for example is 10 s, the frequency difference is 1 Hz. If the duration for 10 revolutions is 100 s, the frequency difference is 0.1 Hz. In this way by just using a stopwatch and measuring the time for 10 revolutions in the polar plot of the phase meter, the frequency shift can be measured. The measurement was repeated typically three to five times during the time interval the transmitter was switched on around the full hours. In this way a total of about 30 measurements could be accumulated during the day. They are displayed in **Figure 2**.

As one can see, there is relatively large scatter in the raw data. However, a clear trend is obvious. The largest positive offset is observed at the earliest time in the morning. The offset decreases with time. It is zero at around noon and after that increases again but with negative values until the end of the measuring period. Interpreted as Doppler shift caused by the movement of the ionospheric layer responsible for the reflection of the space wave sent by DK7XL and received by DL2MDQ 306 km apart, it means that after sunrise the layer is moving downward during the morning hours with decreasing velocity, staying at constant height around noon and afterwards moving upwards with increasing velocity. The effect is of course well known. It describes the building up of the F_1 layer during day time and merging with the F_2 layer again during evening and night time.

Information from Ionograms

To confirm the ideas behind the interpretation of our findings, we inspected the ionograms measured at the branch office of the Leibniz-Institute for Atmospheric Physics in Juliusruh **[6]**, Germany, the metering station located in grid JO64qp, only about 60 km away from the DL2MDQ site. Being so close to our stations and the signal path in our experiment, we expected helpful information to understand and to support our findings. The ionograms are automatically generated at this institute and evaluated by means of the Lowell Digisonde DPSD4 **[7]** and are published many times a day. We inspected about 40 to 50 ionograms as measured during the day of our own measurements. **Figure 3** shows the height variation as function of time.

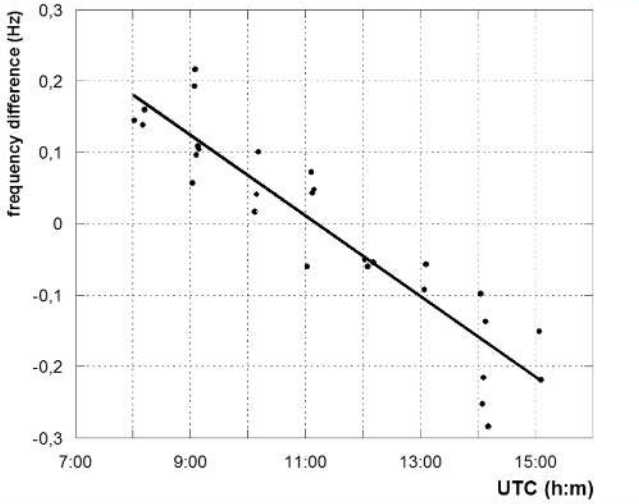

Figure 2 — Frequency differences as measured during the day. Measurements were conducted within about 10 minutes at full hours. Despite the large scattering a clear trend is obvious: the difference is largest in the morning, it is zero around noon and increases again with opposite sign in the afternoon.

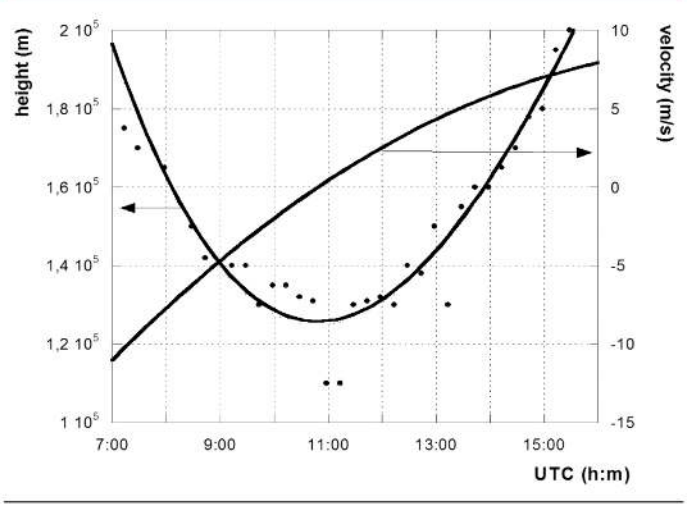

Figure 3 — Height variation as function of time (left scale) as deduced from about 30 ionograms provided during the day (dots). The full line gives a 3rd order polynomial fit to the points manually determined from ionograms. The second curve (right scale) gives the corresponding velocity as calculated via the time derivative of the height function.

The ionograms give information on the height of the reflecting layer for given frequency and for vertical irradiation conditions for both O- and X-modes, from which the height of the reflecting layer as function of frequency is derived. For our propagation geometry as given in **Figure 1**, the 3530 kHz carrier is irradiated under an angle of about 45°. Thus we need to look for the cut-off height for vertical irradiation of about 2500 kHz. If the maximum usable frequency (MUF) for perpendicular irradiation is f_{max} then a signal with higher frequency can be reflected, or rather refracted, at a frequency of about $f_{max}/\cos(\alpha)$ when approaching the ionosphere at an angle α. Vice versa when irradiating at 3530 kHz under 45°, reflection occurs at a height were a perpendicularly transmitted signal of 3530 kHz times $\cos(\alpha)$ is reflected. Thus we have to look in the ionograms for the height of the MUF for perpendicular irradiation of about 2500 kHz.

This information has been extracted by hand from the ionograms. The result is plotted as function of time in **Figure 3**. The layer height varies from more than 200 km in the morning hours. It drops down to about 120 km at noon, reaching the morning height again in the afternoon. The measured points as function of time can approximately be fitted by a polynomial of 3rd order. The height H as function of time t then given by:

$$H(t) = 8.4\times10^{5} - 42.7t + 0.0008t^{2} - 3.9\times10^{-9}t^{3} \quad (1)$$

The corresponding vertical velocity $v(t)$ can easily be calculated with the time derivative of $H(t)$ to obtain:

$$v(t) = \frac{dH(t)}{dt} = -42.7 + 0.0016t - 1.2\times10^{-8}t^{2} \quad (2)$$

This function is plotted in **Figure 3** as well. As can be seen, the vertical drift velocity $v(t)$ varies from about –10 m/s in the morning to about +10 m/s in the afternoon.

The expected Doppler shift f_D for given velocity of the reflecting layer $v(t)$ can be calculated applying the formula:

$$f_D(t) = -2f_s v(t)/c \quad (3)$$

with the propagation speed $c = 3\cdot10^{8}$ m/s, and our signal frequency $f_S = 3530$ kHz.

Equivalently for a given shift $f_D(t)$, the velocity of the reflecting layer $v(t)$ is:

$$v(t) = f_D(t)c/(2f_S) \quad (4)$$

This last expression has been applied to the Doppler shift f_D as measured during the day given in **Figure 1** and compared with the velocity $v(t)$ as derived from the ionograms (**Figure 3**). The result is given in **Figure 4**.

As can be seen, the agreement is good given the fact that the Doppler shifts are measured by hand in a very simple way, measuring phase change in time and applying just equipment available today to a radio amateur.

Simple Model

The propagation model applied so far is very simple. We had in mind a kind of geometrical optics model, the carrier sent and reflected at the ionosphere at a cut-off layer like a mirror. In addition we were using just the vertical drift velocity as deduced from the ionograms to determine the Doppler shift.

A first refinement can be applied by considering the velocity component into the direction to the observer, which is the vertical velocity $v(t)$ times the cosine of the angle α as defined in **Figure 1**, $v(t)\cos(\alpha)$. Just this component is responsible for the Doppler shift, and this is the shift we are measuring in the experiment. The angle depends on half the distance between transmitter and receiver, which is about 150 km, and on the height $H(t)$ of the reflecting layer; $\alpha(t) = \arctan[150/H(t)]$, with $H(t)$ in km. Thus the angle itself is a function of time t. The angle is smallest in the morning when $H(t)$ is large, and maximum when lowest. The cosine term modifies the expression for the Doppler shift resulting in,

$$f_D(t) = -[2f_s v(t)/c]\cos[\alpha(t)] \quad (5)$$

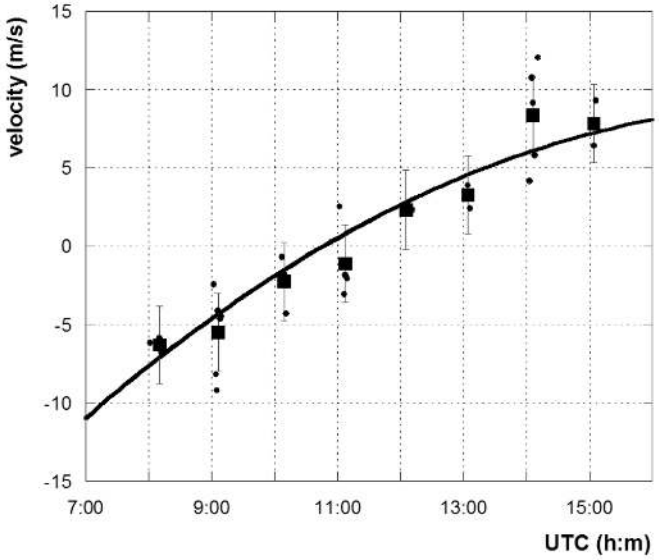

Figure 4 — Velocity as derived from the height variation based on the ionograms (line) in comparison to the velocity as calculated applying Eq (4) to the measurements of the Doppler shift as given in Figure 2. The individual measurements are given by the dots, their average value given in squares. The bars are estimated errors of the measurements.

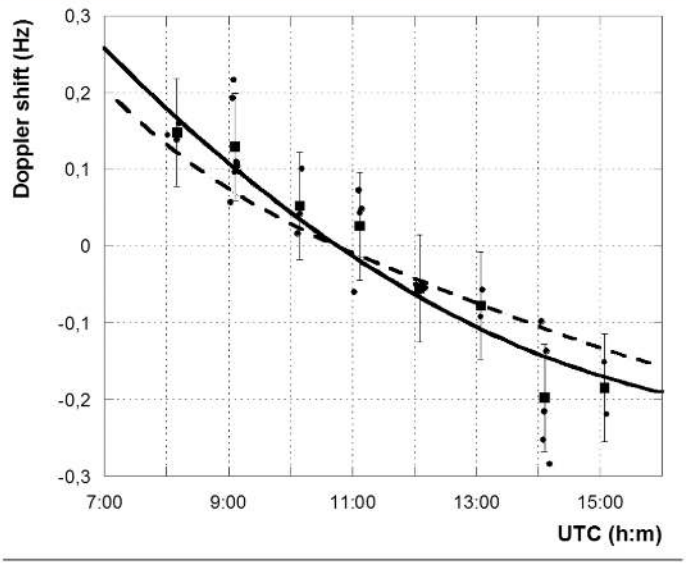

Figure 5 — Measured Doppler shift (dots) and the averaged values (squares) together with the Doppler shift as calculated using v(t), the vertical drift velocity (solid line). The dashed line gives in comparison the calculated Doppler shift considering the velocity component into the direction of the observer. Within error bars, the agreement is still reasonable.

Considering the proper geometry reduces the shift with respect to that calculated on the basis of the ionograms. The result is shown in **Figure 5**.

Discussion and Conclusion

Figure 5 shows that the agreement gets worse when refining the model. However, the error bars of our measurements are relatively large. In addition, we did not discuss at all the error bars of the manually extracted height values of the reflecting layer from the ionograms and our fit to those values, which is difficult. The simple mathematical treatment suggests higher accuracy than is really present. Nevertheless the accuracy and the agreement is good enough to demonstrate the daily shift. The order of magnitude of the drift velocities as derived is in agreement with values given in the literature **[8]**. Detailed measurements are given there for the drift velocities as function of day time with special attention to dawn and dusk hours where maxima of the drift velocity are found. Values vary during the year, they depend on solar activity and geomagnetic activity as well as on latitude.

Basically our simple measurements reproduce qualitatively — quantitatively within a factor of two — what is published in the scientific literature: downward drift in the morning, upward in the afternoon, zero around noon time, and stable conditions during the night. Possibly our report on these early measurements can interest communication experimenters to carry out measurements of this kind observing WWV signals with the aim of exploring in more detail the daily and the seasonal variations of the drift phenomenon.

Acknowledgement

We are grateful to Jens Mielich of the Leibniz-Institute for Atmospheric Physics in Juliusruh, Germany, who has provided us with the ionograms measured during the day of our own experiment.

Hans J. Hartfuss, DL2MDQ, is a licensed ham operator since 1970. He is interested in ionospheric physics, in radio astronomy as well as in ham radio technology. Since Gerald Youngblood's, AC5OG, QEX *series of papers in 2002 he has been an inspired user of SDR technology. He retired from scientific research in plasma physics and fusion research and from teaching at the University Greifswald, Germany. Hans is author of many scientific papers in plasma diagnostics, and is author of the physics text book "Fusion Plasma Diagnostics with mm-Waves."*

Klaus Lohmann, DK7XL, joined ham radio in 1974. His main interest for the first 20 years was short antennas for HF-mobile operations. In 2001 he became an SDR enthusiast and finally worked for 10 years as EU-Representative for FlexRadio Systems. He is now retired and enjoying ham radio with focus on SDR.

References

[1] K. Collins, KD8OXT, D. Kazdan, AD8Y, and N.I A. Frissell, W2NAF, "Ham Radio Creates a Planet-Sized Space Weather Sensor Network," ARRL *QST* Aug. 2021, p 55.

[2] K. Collins, A. Montare, N.I Frisell, and D. Kazdan, "Citizen Scientists Conduct Distributed Doppler Measurement for Ionospheric Remote Sensing," IEEE Geoscience and Remote Sensing Letters; **https://ieeexplore.ieee.org/document/9377452**.

[3] R. Lindquist, "Product Review: FlexRadio Systems FLEX-5000A HF/50 MHz Transceiver," ARRL *QST* July 2008.

[4] H. Hartfuss, DL2MDQ, and J. Sachtleben, DD6UJS, "The Surplus 10 MHz Rubidium Frequency Standard LPRO-101, DATUM/EFRATOM in the Ham Shack, Packet Status Register, 110, 16 (2010), **openhpsdr.org/wiki/images/8/86/Rb-Normal_paper_20.10.09.pdf.**

[5] **https://www.flexradio.com/software/powersdr_v1-18-6_installer/** and **https://www.flexradio.com/documentation/flex-5000-owners-manual/**. For up-to-date PowerSDR see **https://ke9ns.com/flexpage.htm**.

[6] Leibniz-Institute of Atmospheric Physics, Kühlungsborn, Germany, **https://www.iap-kborn.de/en/home/**

[7] **https://www.digisonde.com/**.

[8] D. Kouba and J. Chum, J. Space Weather Space Clim. 8, A29 (2018), **https://doi.org/10.1051/swsc/2018018**.

Errata – *QEX* Jan./Feb. 2021

In Eric P. Nichols, KL7AJ, "Self-Paced Essays — #9 Angular Frequency," *QEX* Jan./Feb. 2022, p. 34, bottom of column 1, we should have stated, "We know that Circumference/Diameter = π, regardless." Also in the top of column 2, the correct phrasing is, "In like manner angular frequency ω can often …" Thanks to Joseph Sybille, N5AYR, who spotted the errors.

Richard H. Grote, K6PBF

547 Hilbar Ln., Palo Alto, CA 94303-3026; **k6pbf@arrl.net**

ATWIFI Clock / Weather / Solar Display

Derive and display data from internet sources using this Arduino based project.

More than a year ago I set out to replace the analog "guts" of a cross-meter SWR/power meter that I had picked up at a swap meet. It contained an Arduino circuit with a four-line LED display auxiliary to the meter. I realized that this LED SWR display was useful only while I was transmitting, and I started thinking about other uses for such a display. Pretty soon I set aside the SWR/power meter project and focused on a new Wi-Fi based UTC clock/weather/solar display (**Figure 1**). While there are more elegant solutions for much of this functionality **[1]**, my display is simple and costs about $25. It's great addition to my shack.

Figure 1 — The Wi-Fi based UTC clock/weather/solar display.

Using information downloaded from internet sources, the 4-line LED display shows UTC time and date, local temperature, barometric pressure, wind speed and direction, and key current solar conditions (**Figure 2**). The solar conditions displayed are sun spot number, solar flux index, A and K indexes, and solar wind.

In an earlier version of the display, electron and proton flux were shown instead of solar wind, but I found solar wind interesting to watch and surprising to me as it varies considerably from day to day. I also download and check electron and proton flux and X-ray information. If they are above a level that might cause compromised band conditions, I flag that incidence with an *ALERT* on the display, see **Figure 2**.

Hardware – the Easy Part

The principal components of the display are an Arduino Nano, an ESP-01 8266 Wi-Fi module, and a four line by 20-character I2C display. Since this project started as a clock, I considered other time sources such as a real time clock (RTC) or GPS receiver. I've used RTCs before and didn't want to fool around with setting the time and dealing with time drift. The GPS was a viable solution, but I liked the idea of harvesting other information from the internet and settled on an ESP8266 module, ESP-01, which is low cost and amazingly powerful. Since the ESP-01 requires 3.3 V, and the 3.3 V internal supply from the Arduino won't supply sufficient current, a separate 3.3 V is regulator is required.

The complete schematic is shown in **Figure 3**. The display connects to the Arduino with a 4-wire interface. Additionally, there are two pins on the display that when shorted, provide backlight for the LCD. I found this backlight too bright in dim ambient conditions and added an automatic brightness circuit in my design with a photocell and some electronics, see the "Backlight Control" circuitry in **Figure 3**.

Software — a Bit More Challenging

The program — a sketch in Arduino vernacular — is available on **arrl.org/QEXfiles**, looks pretty simple at first

Figure 2 — Display showing an ALERT.

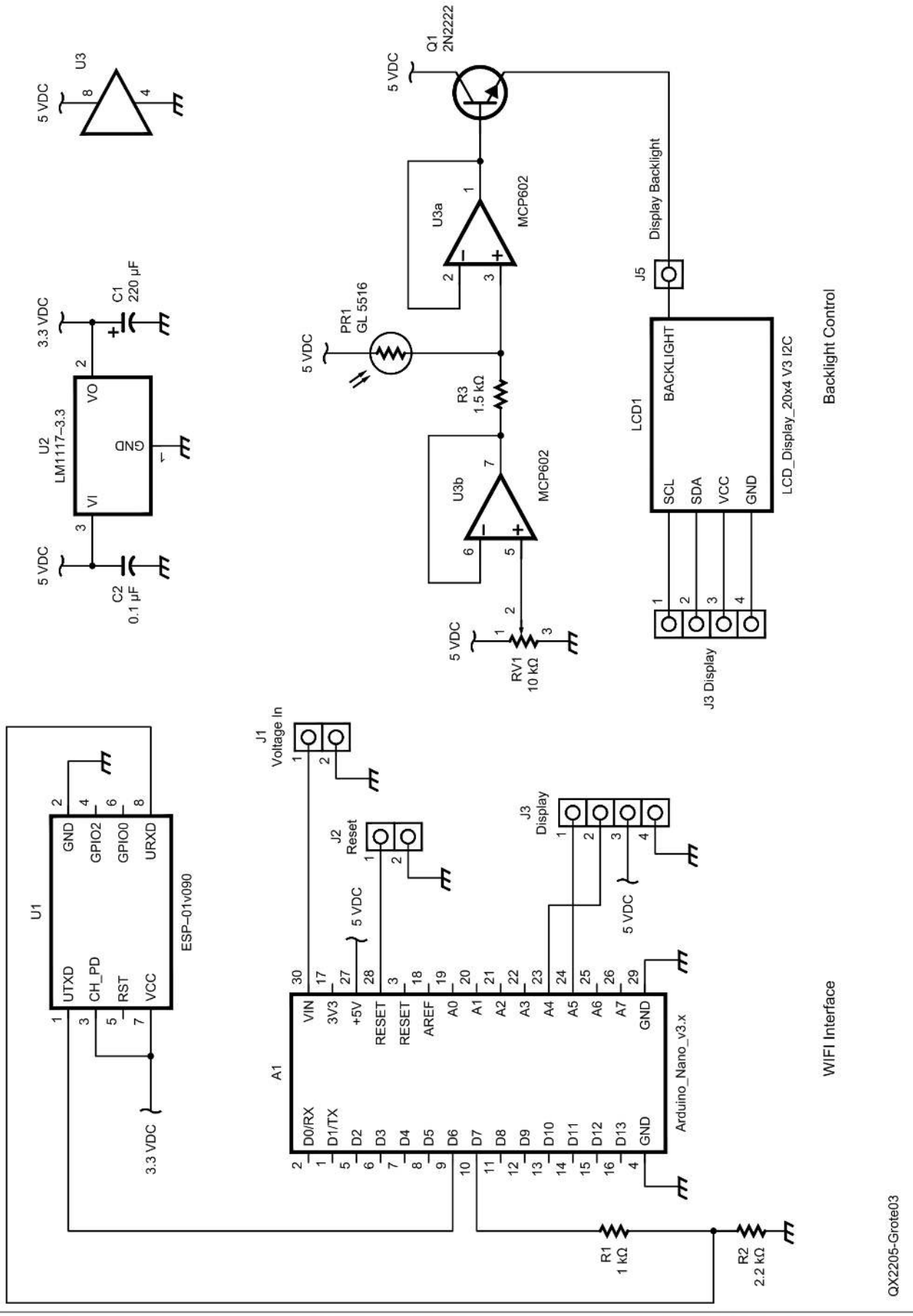

Figure 3 — Schematic diagram of the Wi-Fi based UTC clock/weather/solar display. The BOM is Table 1.

examination. After an initial set up, the sketch loops through calls to functions to check and update the time every 10 seconds, the weather every 10 minutes, and the solar conditions every hour. I wrote specific routines to process these updates that depend very heavily on a Wi-Fi library to communicate through the ESP-01 and access internet information.

I moved back and forth between the Arduino IDE and Visual Studio Code with Platform IO for the development platform and finally settled on the latter because the development tools it brings make things so much simpler. Managing memory usage was a constant battle throughout the development of the display. A small change to the program would suddenly cause random characters to appear on the display. The Nano has 2 KB of memory and I found that if much more than 75% of the memory is used, there often would be problems. I spent a great deal of time making things as simple as possible, and minimizing memory usage.

Talking to the Internet

The ESP 8266 is a very powerful chip. It is a dual core processor with a full internet protocol stack so that it can access a Wi-Fi node and through it gain access to the internet with minimal control overhead from the Arduino. It has become very popular for Internet of Things (IOT) applications. The ESP 82686 is packaged in several different form factors. I decided on the ESP-01 because it was readily available and inexpensive. Of course, things are more complicated than just buying a part. I needed to find an Arduino library that would support the functions I settled on the WiFIEspAT library. This library relies on specific ESP 8266 firmware. Burning required firmware **[2]** is a straightforward, but requires care and a small fixture that connects to a USB port of a computer. Details for this operation are described in a separate document at **arrl.org/QEXfiles**.

The ESP-01 is instructed by the Arduino to connect to a webpage and it then starts streaming information from that webpage to the Arduino on a serial interface. It doesn't take much data to swamp the small memory of an Arduino so it is necessary to pull out the desired information on the fly. After trying some available Arduino library solutions for this data separation (parsing), I ended up writing my own function routine to search for data streaming out of the ESP-01 and grabbing what I wanted based on a few search criteria.

As everyone who surfs the web knows, web pages sometimes don't load or just hang. This is true for this display as well. Largely though experimentation, I found what would happen when connections failed. I wrote work arounds to adjust to these situations. In most cases, I just skip the update and wait for the next update cycle. Once in a while the connection will hang. When this is detected, I restart the display. This doesn't happen often, but once in a while the display will go blank and "Connecting to WIFI" is printed to the screen. This happens also when the Wi-Fi goes down. After about a minute everything is back to normal. I brought out a pair of pins that when shorted will reset the Arduino. This doesn't happen very often, but it may be necessary. Of course, you can use the reset button on the Nano as well.

Data Sources

Obtaining solar condition information was made very easy thanks to the wonderful online resources **[3]** of Paul Herrman, NØNBH. Paul's propagation banners appear on multiple ham websites. Paul includes in his website an Extendable Markup Format (XML) format link that provides access to his solar data, which in turn is easily accessed and parsed. He has requested that this information not be queried more often than once an hour. Since the solar numbers don't change quickly, this is very a reasonable request and was easy to manage in the program. There are several resources that explain the relevance of these numbers **[4]**.

There are multiple weather information sources on the web. I settled on **openweathermap.org** for convenience to use and because I live in an area with multiple microclimates, it is the most accurate for my location. Use of their service requires a license, but it is free as long as you make no more than 60 queries per hour. I planned on checking weather every 10 minutes, so this wasn't a problem. Their information is also available in XML format.

The most obvious time source is the Network Time Protocol (NTP). It is very easy to build a UTC clock using the Arduino NTP library **[5]**. However, I learned quickly, at least with my software skills, that while I could make the NTP clock work, I couldn't then use the Wi-Fi internet connection for other purposes. Since every downloaded web page has a UTC time stamp associated with its header, I decided it was convenient to download a page, parse the header to get the current time and date. I choose **https://jsonplaceholder.typicode.com/** which serves as a testing API for software development. The site claims that they serve 1.8 billion requests per month so I assumed that they could handle a few additional hits from me. I didn't care whether the clock is accurate to the second, so I make a call about every 10 seconds to this website and receive the header string with its accompanying UTC time and date stamp. It is a relatively easy task to get the current UTC date and time from that string.

Putting It All Together

Build the display using these steps.

1) First constructed the circuit. My first pass was on a solderless breadboard. Since the spacings of the pins of the ESP-01 don't work on these breadboards, I found an adaptor (Addicore AD-BB-ADTR) that makes connections possible. Since there are

Table 1 – Bill of Materials.

Part #	*Value*	*Description*
A1	Arduino Nano v3.x	MCU Module
C1	220 µF	Capacitor
C2	100 nF	Capacitor
J1	Voltage In	Connector, 01x02
J2	Reset	Connector, 01x02
J3	Display	Connector, 01x04
J5	Display backlight	Connector, 01x01
PR1	GL 5516	Photo
Q1	2N2222	Transistor, BJT (or 2N3904)
R1	1 kΩ	resistor
R2	2.2 kΩ	resistor
R3	1.5 kΩ	resistor
RV1	10 kΩ	potentiometer, trimmer
U1	ESP-01v090	ESP 8266: ESP-01v090
U2	LM1117-3.3	Regulator, Linear: LM1117-3.3
U3	MCP602	Amplifier, Operational: MC33078
Display	4x20 I2C	Serial IIC/I2C/TWI 20X4 Character LCD Module

relatively few connections in the design, a point-to-point breadboard is not difficult. I also laid out a PCB (see **Figure 4** and the **arrl.org/QEXfiles** web page).

2) The BOM is in **Table 1.** I acquired all of the components from various eBay vendors. I purchased an ESP-01 from each of three different vendors and they all perform well when properly flashed with the required software.

3) If a clone Arduino Nano is used, then it may be necessary to load a USB driver. This website is very useful for how to get and install this driver: **https://www.instructables.com/Arduino-Nano-USB-Not-Recognizing-Fix/**.

4) The Arduino IDE must be installed on the host computer (there is a lot of information on the web on how to do this). The following libraries must be installed:

(a) SoftwareSerial.h – standard IDE driver,

(b) LiquidCrystal_I2C.h, see **https://github.com/johnrickman/LiquidCrystal_I2C/**.

(c) WiFiEspAT.h, see **https://github.com/jandrassy/WiFiEspAT/**.

(d) The Wi-Fi Clock/Weather/Solar Arduino program is found in the **arrl.org/QEXfiles** web page.

5) I've found that not all 4-line displays have the same I2C address. In my case the green was one address and blue was another. I found a useful tool in the Arduino Project Hub that helps discover the I2C address of the display, or any other I2C device connected to the Arduino: **https://create.arduino.cc/projecthub/abdularbi17/how-to-scan-i2c-address-in-arduino-eaadda?ref=user&ref_id=1134675&offset=1**.

6) A license from **Openweathermap.com** is required. Go to this website and subscribe to "Current Weather Data." It is simple to setup the free API account. After the setup is competed, *Openweathermap* will issue a pass code. We must enter this pass code in the sketch.

7) Load Conditions display into the Arduino IDE. The following modifications to the code must be made:

(a) Find the correct I2C address found in Step 4 and make sure that this is the address used in the *LiquidCrystal_I2C* definition line. This is in the first 20 lines of code.

(b) Edit Wi-Fi constants to include your Wi-Fi SSID and pass code. This is in the first 70 lines of code.

(c) In the *void weather()* routine insert the API Key you obtained Step 6.

Search for *void weather()* and the key, and following location information is entered near the end of the function.

(d) Edit the constant string location in the Weather Reader void to reflect your QTH. I left my QTH as an example in the sketch. I found that I could experiment in a standard browser with the *openweathermap* call parameters to get the weather data needed.

(e) At this point the sketch is ready to upload and the clock should start operating. Initially "Connecting to WIFI" is displayed, but then in fairly brief sequence the date/time appears with 0° temperature, followed by the weather information, which should then populate the temperature, and then the solar conditions. Now the display will run continuously.

8) Adjust the contrast potentiometer on the back of the display until displayed characters are clear. If the backlight feature is being used, the display must be powered by an external dc voltage of 7 to 12 V. The backlight control potentiometer should be adjusted so that the display in a dim environment is at desired brightness. Five-volts dc is adequate or the circuit can be powered through the microUSB port of the Arduino if the backlight control circuit isn't used.

9) Packaging. The circuit is so small that there are many options to house the display. Initially I build a little wooden box, but decided that it was still bigger than needed. Finally, I mounted it on the back of a Plexiglass stand that I found on eBay; **https://www.ebay.com/p/942136956**. I mounted a small piece of Plexiglass on the back of this stand and then mounted the circuit board onto this Plexiglass.

There are many joys to be found in amateur radio, but for me the greatest rewards are using something that I've built. I didn't start out to build this display, but it has become my favorite all time project. Now that sunspots are on the rise, I get up every morning to look at the display and decide whether I want to go outside or stay inside and play radio.

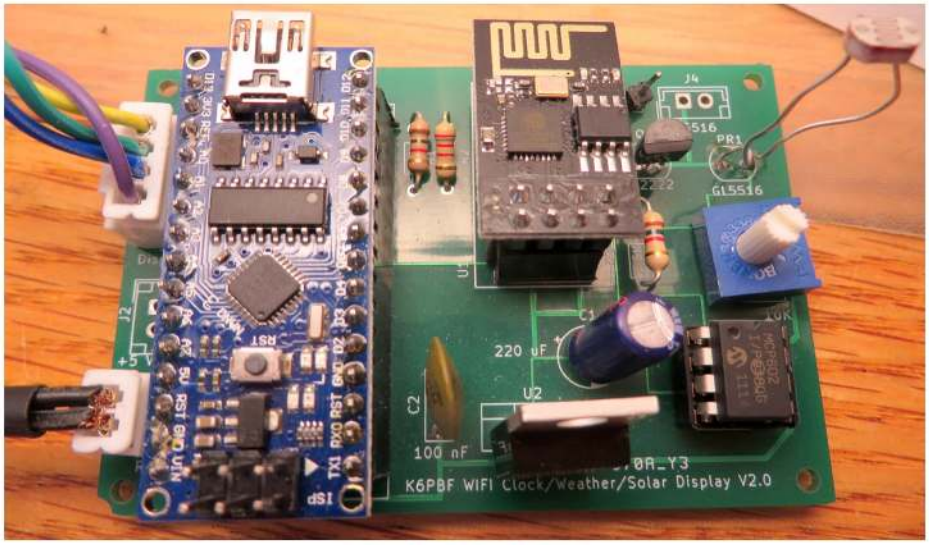

Figure 4 — Board image.

[Photos by K6PBY.]

Richard Grote, K6PBY, grew up with an early interest in electronics, building crystal sets and eventually an "Ocean Hopper" from Allied Radio. Lacking a mentor, he never got an amateur license when he was young. The early interest in electronics led to BSEE and MSEE degrees from University of Kansas and Stanford respectively. He started as a design engineer in an instrumentation lab of Hewlett Packard and progressed into management. After a dozen or so years he moved over to the computer side of the company, and was involved with personal computers where he managed R&D development organizations. After retirement he found a mentor, and finally got his ham license. In the last 10 years he has been making up for lost time, chasing DX, POTA, QSO parties, and getting his hands dirty building things. In addition to the ham hobby, he's the neighborhood fixit-guy, and is busy watching over grandchildren and building them wooden toys. Richard has been married 50 years, has two daughters, and three grandkids.

References

[1] E. Downey, WBØOEW, "HamClock," *QST*, Oct. 2017.
[2] Burning firmware, see: *ESP 8266 Firmware* folder in **arrl.org/QEXfiles**.
[3] P. Herrman, NØNBH: **hamqsl.com**.
[4] See **www.hamqsl.com/solar2.html#glossary** and "Solar Banners — A Propagation Resource", *QST*, Feb. 2014.
[5] Build a UTC clock using the Arduino NTP library: **https://www.arduino.cc/reference/en/libraries/ntpclient/**.

Eric P. Nichols, KL7AJ

AlasKit Educational and Scientific Resources, 3763 Lyle Ave., North Pole, AK 99705; **kl7aj72@gmail.com**

Self-Paced Essays — #11 Reactance

Reactive components store energy, while resistive ones dissipate energy.

We've suggested before that there are actually only three components in all of electronics: resistors, capacitors, and inductors. Even active devices like transistors and vacuum tubes are nothing more than controlled resistors. With this in mind, it is astonishing how complex and elegant electrical networks and circuits can be.

In the previous essay, we approached the concept of reactance, which in its simplest form can be defined as the opposition to current flow presented by one or more components.

As we will discover, the amount of opposition to current flow presented by a capacitor or an inductor is frequency dependent. For a reactive component, like a capacitor or inductor, this opposition to current flow is called reactance, and its unit is the ohm — not too surprisingly. A "normal" ohm and a reactive ohm are dimensionally equivalent — refer to *Essay 9* for a description of dimensional equivalence. Sometimes reactance is described as frequency dependent resistance, but one needs to be careful with this "definition" because there are *true* frequency dependent resistances such as skin effect, which we will discuss later in this series.

What really differentiates a reactive component from a resistive one, is whether energy is stored or dissipated. A reactive component only stores energy; it does not dissipate any energy, or convert any energy into heat. We do need to emphasize that we are talking about ideal components; one must always understand the ideal before working with the real. Conversely, a non-reactive component — such as a resistor — stores no energy, but converts it all into heat.

There are two possible "storage tanks" in electronics: either an electric charge, or a magnetic field. Capacitors store energy as an electric charge, and inductors store energy in a magnetic field. All the energy in these "storage tanks" is fully recoverable. Energy converted into heat in a resistor is lost forever.

Now, if you recall the last example in *Essay 10*, you saw that the voltage applied to a capacitor and the current passing through the capacitor don't occur at the same time. If, instead of a dc voltage source, we have an ac generator, we would also see a timing offset between voltage and current, but it would be now much more definable. In a circuit consisting of only an ac voltage source — remember a voltage source has no internal resistance — and a capacitor, the phase difference between voltage and current is always 90°. The current leads the voltage by 90° (or $\pi/2$ radians). This amount of phase shift is independent of frequency.

Similarly, if you apply an ac voltage to an inductor, the voltage across the inductor, and the current through the inductor will be shifted by $\pi/2$ radians, but in the opposite direction, with voltage leading the current. This 90° phase shift is also independent of frequency.

The familiar mnemonic "ELI the ICE man" will remind you which direction the phase is shifted. In an "*L*" the *E* leads the *I*, and in a "*C*" the *I* leads the *E*.

The fact that the phase shift is independent of frequency, while the reactance — opposition to current flow — is frequency dependent gives us some extremely useful properties to play with.

Although this is probably old news to most of you, we should re-iterate the formulas for reactance. For a capacitor, the capacitive reactance, $X_C = 1/(2\,\pi\,f\,C)$, is in ohms, f is in hertz, and C is in farads. For an inductor, $X_L = 2\,\pi\,f\,L$, where X_L is in ohms, f is in hertz, and L is in henry.

Because resistance and reactance are dimensionally equivalent, but are different in character — resistance is dissipative, and reactance is energy storing — it is convenient, if not absolutely necessary, to plot these values on a two-dimensional graph, to make sense of how they interact.

I've discovered that 1 is an extremely useful number. Just to keep things simple, let's calculate the reactance of a 1 H inductor when driven by an ac voltage at 1 Hz. Using our formula $X_L = 2\,\pi\,f\,L$, we can work out in our heads that the reactance is $2\,\pi = 6.28$ ohms. There is rarely a need to work out π to more than three significant digits in anything we do in amateur radio.

We seldom have an inductor just flapping in the breeze by itself, so it helps to connect it to something. Why don't we put a 1 ohm resistor in series with our inductor, and drive the whole thing with a 1 Hz ac source? What do you suspect the total opposition to current flow will be? Hint: it won't be 7.28 ohms. Life is more interesting with reactive components. So, let's bring out our promised two-dimensional graph and see if we can make sense of this.

I use a free program called *Octave*, which is closely related to *MATLAB* for doing all kinds of interesting graphs and such. *Octave* has a bunch of really handy Polar-to-Cartesian and Cartesian-to-Polar conversion and display tools. We'll be using

it a lot for the duration. It also has a lot of wonderful color features, which, alas, we can't show in the printed *QEX* black and white format. If you want to see the color versions of these plots, feel free to email me.

The graph of **Figure 1** shows us both the Cartesian (x and y) grids as well as a Polar grid. We'll plot resistance on the horizontal axis, and reactance on the vertical axis. Inductive reactance is anything above the origin, and capacitive reactance is anything below the origin. By convention, we use j Im{Z}to indicate the reactive or imaginary part of an impedance, and Re{Z} to designate the real part of the impedance, as we will explore shortly. The Polar plot will show us phase angle, with 0° always oriented due east. The quadrants of the graph are numbered sequentially counterclockwise from 0°. Almost all our impedance calculations will be in the first and fourth quadrants. However, there is such a thing as negative resistance, which we will explore later on. But for most of our work a "half-graph" will be sufficient. The scale of this graph is ohms, in any direction. Remember that we can do this because reactance is dimensionally equivalent to resistance.

So, I've placed the end point of the arrow in **Figure 1** at our two coordinates; to the right one unit from the origin for our resistance, and 6.28 units up from the origin for our inductive reactance. To avoid getting too cluttered right off the bat, I've omitted the individual x and y vectors.

A couple if things immediately stand out. First, we have the total length of the arrow, which is about 6.36 Ω. Second, we have the phase angle — the angle between voltage and current — which is 81° counterclockwise from due east. This is our complex impedance, Z. We can use either a protractor, or a little trigonometry to find this angle to greater accuracy than we can by glancing at the plot. For a complex circuit, the phase angle is the arctangent of the reactance over the resistance, which is $\tan^{-1}(6.28/1) = 80.952°$. This circuit is almost totally reactive.

Let's apply a known voltage to this and see what kind of power is actually consumed. For any complex series circuit, to obtain our current we can simply substitute Z for R in our Ohm's Law formula. If we apply 100 V to the circuit, using $I = E/Z$, we come up with 100/6.36 = 15.7 A. We can simply multiply current times voltage,

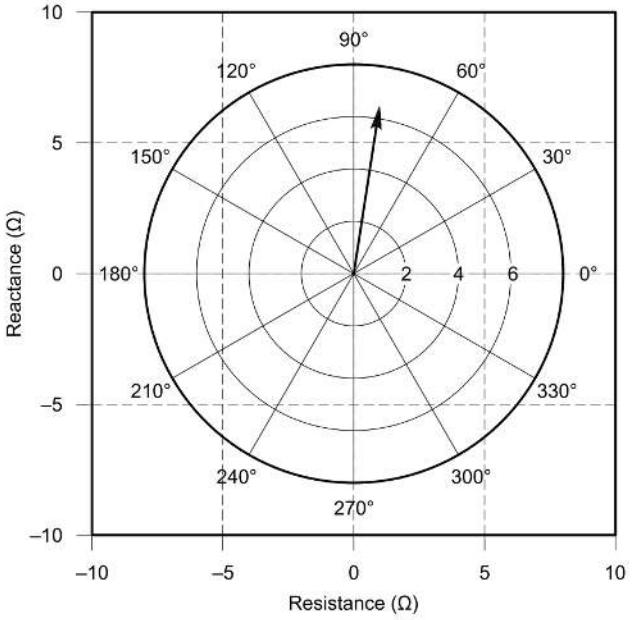

QX2205-Nichols01

Figure 1 — A complex impedance displayed in Cartesian and Polar coordinates.

which gives us 15.7 × 100 = 1570 W. That's a lot of watts. Now, if you've followed this essay series for a while, you know that I always like to figure things out by at least two different methods and see if we come up with the same answer. I'm very big on sanity checks.

So, let's calculate the resistor's power directly. We know that in a series circuit, the current is the same anywhere, so we know we can figure out the resistor's power by I^2R. $15.7^2 \times 1$ gives us 246 W. Hmm... that's interesting. Where did the other 1324 W go? If you said the inductor, remember reactive components dissipate no power, they simply store energy; and we *are* working with ideal, perfect components at this point.

What we have encountered is the difference between true power and apparent power. Apparent power is simply voltage times current. True power is the apparent power times the power factor, which is the cosine of the phase angle. The cosine of 80.952° is 0.157 and 1570 × 0.157 gives us 246 W, plus or minus some loose change. Voila!

The important point here is that power is consumed *only* in a resistive (real) component. Incidentally, the generator in this case is also only producing 246 W. We leave that as an exercise to explain why.

There are a couple of other interesting features of this circuit. We can easily calculate the voltage across the resistor, using a version of Ohm's Law, $E=IR$. It is 15.7 V. We can also figure out the voltage across the inductor, using $E=IX$, which is 15.7 × 6.28 = 98.6 V. Add 15.7 to 98.6 V and we get 114.3 V. How is the sum of the inductor voltage and the resistor voltage greater than the supply voltage? No magic, it's the stored energy that makes this possible, and we find this situation occurs with either inductive or capacitive reactance. The greatest increase in voltage at the "midpoint" of the circuit, where there's a resistor and a reactance in series, occurs when X is equal to R, in which case you get a 1.4-times increase as well as a 45° phase shift.

Now for our homework problem. You have a 12 V, 25 W automotive lamp that you want to power from a 120 V, 60 Hz, wall outlet. You can reduce the voltage to the lamp in an efficient manner by putting an inductor in series with the lamp. What value of inductance do you need to make the lamp happy?

In the next installment, we'll consider capacitive reactance, and work our way towards the all-important concept of resonance.

Upcoming Conferences

Microhams Digital Conference 2022

May 7, 2022

Virtual

www.microhams.com /mhdc-2022

15th Annual Microhams Digital Conference, sponsored by the Microsoft Amateur Radio Club (Microhams) will be live streamed on YouTube, May 7, 2022. This conference has a focus on digital communications, and offers a variety of topics across a range of skill levels. Our motto is "Inspire, Inform and Educate." This year the conference will be streamed and at no charge (donations welcome). The latest updates will be published on the Microhams web site. A chat channel will be available to ask questions of the presenters, and will be addressed at the end of the presentations. To provide a more interactive experience, there will be a Zoom breakout room available at the end of the session where the presenters can hang out and answer questions in person. The conference will be recorded on YouTube and will be available for viewing later. See website for details.

Aurora 2022

June 4, 2022 (9 AM – 5 PM CDT)

Plymouth, Minnesota

www.nlrs.club/#Aurora%20 Conference

Aurora 2022 will take place June 4, 2022, from 9 AM through 5 PM CDT. This year's venue is the West Medicine Lake Community Club, 1705 Forestview Lane North, Plymouth, Minnesota. Aurora, the largest annual gathering of weak-signal VHFers in the Upper Midwest, is the annual meeting of the Northern Lights Radio Society.

In the morning hours, the club runs an outdoor antenna range from 0900 to 1130 (weather permitting). The morning also allows for socializing, show-and-tell, and casual demonstrations. Members are on their own for lunch. The technical programs start at 1300 and typically run through 1700 – 1730. If you have a weak signal VHF topic that is of interest to you, or that you would like to present, please contact our Technical Chairman, Jon Platt, WØZQ, **w0zq@aol.com**. Aurora also features a poster session. See website for details.

CSCC 2022

July 19 – 22, 2022

Platanias, Chania, Crete Island, Greece

www.cscc.co

26th International Conference on Circuits, Systems, Communications and Computers is planned to take place as a hybrid conference (face-to-face and online) in Crete, Greece, July 19 – 22, 2022. See website for details.

Central States VHF Society 2022

July 22 – 23, 2022

La Crosse, Wisconsin

http://2022.csvhfs.org/

The 54th Central States VHF Society 2022 Conference will be held at the Radisson Hotel, La Crosse, Wisconsin, July 22 – 23, 2022. This year's event will have technical presentations, antenna range, noise figure lab, rover row and dish bowl, Thursday evening social activity, Friday evening trade-fest, dealer room, hospitality suite for evening socializing, fun family activities, and a closing banquet with a guest speaker and a prize table. See website for details.

Get Ready for Field Day—June 25-26!

TransWorld Packages

TransWorld antennas are small and portable, yet provide superb performance and durability. DX Engineering has created several packages including the 5-Band Explorer combo, which delivers 20-10M coverage with manual bandswitching. It comes with a portable quadrastand, basic antenna structure, and travel bag. Band-Specific Solo Explorer packages are available for the 80, 60, 40, and 30 meter bands. Accessories include DX Engineering's center box protective cover. **Enter "TW" at DXEngineering.com.**

samlexamerica KENWOOD ASTRON CORPORATION
ALINCO YAESU AMERITRON

Power Supplies

Make DX Engineering your source for reliable switching and linear power supplies from major brands, including Alinco, Ameritron, Astron, Kenwood, Yaesu, and more. Choose from units with input voltages from 85 to 260 Vac and peak outputs from 10 to 50 amps. **Enter "Power Supplies" at DXEngineering.com.**

Headset and Footswitch Packages

Add greater flexibility to your station! Choose from eight packages that feature a rugged DX Engineering footswitch paired with either a Heil Pro 7 or Elite stereo headset, each loaded with ham-friendly benefits: high rejection of outside noise, articulate audio, exceptional comfort, less listener fatigue, and more. Headset adapter cable sold separately. **Enter "DXE Headset Foot" at DXEngineering.com.**

plasticase NANUK PROFESSIONAL PROTECTIVE CASES RigExpert®

RigExpert Analyzer and NANUK Case Combos

In the field, an antenna analyzer is especially at risk for weather and shock damage. We've paired select RigExpert Antenna Analyzers with perfectly sized NANUK equipment cases. Each case is filled with cubed, sectioned foam for custom configuration. Available separately or in combos. **Enter "Analyzer Combo" at DXEngineering.com.**

Coaxial Cable Tool Kits

Get everything you need to prep and install soldered, crimp-on or Universal Compression F-connectors on your coax. Complete kits include cable strippers, grippers, replacement blades, braid trimmer, cable shears and carrying case. The Ultra-Grip 2 Crimp Connector Hand Tool Kit comes with a ratcheting steel crimper and five die sets for making professional-quality crimps on coaxial and Powerpole® connectors. Individual tools also sold separately. **Enter "Tool Kit" at DXEngineering.com.**

Coaxial Cable Assemblies

These low-loss cable assemblies are available in standard lengths with DX Engineering's revolutionary patented PL-259 connector. Use the online Custom Cable Builder at DXEngineering.com to build assemblies made to your exact specs. DX Engineering's coaxial cable is also available by the foot or in bulk spools. **Enter "DXE Assemblies" at DXEngineering.com.**

Multi-Band Dipole Antenna Kits

Ideal for easy setup on Field Day, these rugged yet lightweight 2,500W power rated antennas are usable to 30 MHz with a tuner balun (available separately). They feature strong and flexible 14 AWG stranded-copper, relaxed PVC-jacketed elements; 18 AWG 300-ohm ladder feedline; center-T support; and end mount brackets.

DXE-WA-070	Antenna, 70' Long for 40M and Up	**$64.99**
DXE-WA-135	Antenna, 135' Long for 80M and Up	**$73.99**
DXE-WA-260	Antenna, 260' Long for 160M and Up	**$89.99**

Coaxial Dynamics AMERITRON DAIWA
DIAMOND ANTENNA ELECRAFT Palstar

SWR/Wattmeters

Measure forward and reflected transmitter power with SWR/wattmeters from top brands, including Ameritron, Coaxial Dynamics, Daiwa, Diamond, Elecraft, and Palstar. Choose from models with true peak and average readings, 20/200/2,000-watt ranges, amplifier bypass for high SWR, high SWR audio alarms, remote sensors, and more. **Enter "Wattmeter" at DXEngineering.com.**

YAESU ICOM KENWOOD ALINCO AlexLoop GAINER Cases iPortable MASTPANT

Get All Your Field Day Gear Right Here!

DX® ENGINEERING

Ordering (via phone) Country Code: +1
9 am to midnight ET, Monday-Friday
9 am to 5 pm ET, Weekends
Phone or e-mail Tech Support: 330-572-3200
9 am to 7 pm ET, Monday-Friday
9 am to 5 pm ET, Saturday
Email: DXEngineering@DXEngineering.com

Ohio Showroom Hours:
9 am to 5 pm ET, Monday-Saturday
Ohio Curbside Pickup:
9 am to 8 pm ET, Monday-Saturday
9 am to 7 pm ET, Sunday
Nevada Curbside Pickup:
9 am to 7 pm PT, Monday-Sunday

800-777-0703 | DXEngineering.com

ON ALL BANDS YouTube

We're All Elmers Here! Ask us at: Elmer@DXEngineering.com
Email Support 24/7/365 at DXEngineering@DXEngineering.com

MAXIMIZE YOUR CAPABILITIES

SteppIR Antenna Systems are designed for performance, period. Each individual element is tuned remotely using an electronic controller, so the antenna is the exact length it needs to be at any given frequency – which results in superior performance and bandwidth. Gone are the days you have to compromise performance by tricking the antenna into thinking it is a different length by using traps, interlacing elements or simply adding more elements. Whether you are a new ham radio operator or have "worked 'em all", we have the antenna for you. Step up to SteppIR – it's a monoband antenna... on every frequency!

- YAGI ANTENNAS
- VERTICAL ANTENNAS
- PORTABLE ANTENNAS
- CONTROLLERS
- OPTIMIZERS
- ANTENNA ANALYZERS
- ACCESSORIES

SMALL FOOTPRINT
BIG DELIVERY

YAGI URBAN BEAM

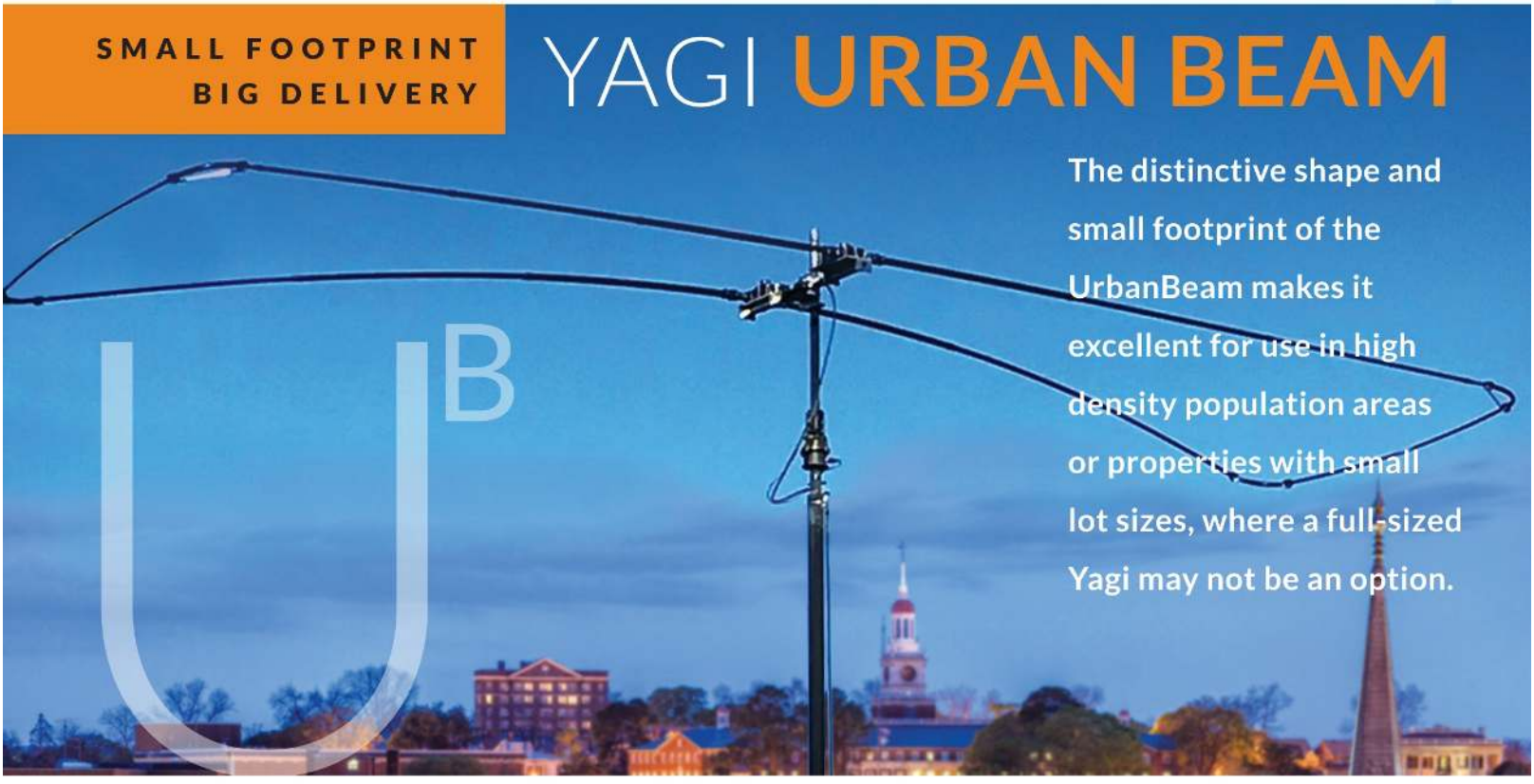

The distinctive shape and small footprint of the UrbanBeam makes it excellent for use in high density population areas or properties with small lot sizes, where a full-sized Yagi may not be an option.

steppIR
COMMUNICATION SYSTEMS

FOR PRODUCT DETAILS AND ORDERING: www.steppir.com 425-453-1910